UNIVERSITÀ DEGLI STUDI DI TRENTO

Facoltà di Scienze Matematiche, Fisiche e Naturali
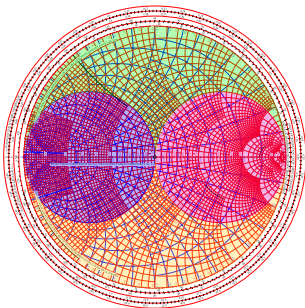
UNIVERSITÄT INNSBRUCK

Institut für Experimentalphysik

Corso di Laurea Specialistica

in Fisica della Materia di Base e Applicata

Final Thesis

Compact RF Amplifier for Scalable Ion-Traps

1st Reader:
Dalfovo Franco
Università degli Studi di Trento

.   **Graduand:**
Gandolfi Davide

2nd Reader:
Brownnutt Michael
Universität Innsbruck

Academic year 2010-2011

Abstract

This thesis reports the investigation and the implementation of a lumped component, radio-frequency resonator used to drive an ion-trap in a cryogenic vacuum environment. The resonator was required to achieve the voltages necessary to trap while dissipating as little power as possible. The cryogenic environment makes the design of the circuit challenging, since Joule dissipations have to be avoided and the components' reliability has to be tested.

With the final resonator a voltage gain of 100 was measured at $5.7\,\mathrm{K}$. Two calcium ions were trapped in a trap driven by this device, evidence of successful resonator operation at low temperature.

Contents

1. Introduction

Quantum mechanics was born to describe the microscopic world of the constituent parts of matter. It is successfully used to explain nuclear reactions, as well as the atomic properties of various elements or molecules. It can provide clues on both ordinary and exotic states of matter, like Bose-Einstein Condensates (BECs) or neutron stars. Physicists, and scientist in general, are used to the extravagances of this strange world, but it is only in the last two decades that technological knowledge has grown enough to be able to engineer the quantum state of individual (or a small number of) particles.

In particular, the ability to manipulate simple quantum systems at will enabled the possibility to use them (and the laws of quantum mechanics) in applied sciences like Information Theory and Computation Theory. These new sciences are called Quantum Information (QI) and Quantum Computation (QC), respectively [1, 2]. In both of these new branches, the fundamental building block is the quantum bit, or qubit, where the logical state $|0\rangle$ or $|1\rangle$ is encoded in the quantum state of a two-level system. The new features (with respect to classical information theory) introduced by quantum mechanics are the existence of *superposition* of logical states and the existence of the *entanglement*. The term superposition refers to the simultaneous existence — weighted by some complex amplitude coefficients — of all the logical states, which in classical information theory are mutually exclusive. Entanglement is the non-local instantaneous quantum correlation of more than one individual particle. This additional complexity allows quantum systems to be used in simulating and solving more complex problems. It is the accurate engineering of superposition and entanglement [3] which makes quantum computation special, though much of the time maybe counterintuitive [4].

The first notable proposal for the use of a quantum computer was made by Richard Feynman in 1982 [5]. He proposed — or better, conjectured — the use of a quantum system to simulate efficiently some class of physical problems which cannot be efficiently simulated by classical means. By now, almost thirty years later, a fully scalable universal quantum simulator does not exist, but some problem-specific simulators are built and have given the first results [6, 7, 8, 9]. In the 1990s the theoretical background of QC grew rapidly, with the formulation of several quantum algorithms and the proposal of several suitable two-level quantum systems. The most famous algorithms, which can provide more efficient calculations, are the search of an unsorted database [10] and prime factorization [11]. During the 2000s, proof-of-principle demonstrations of many of these algorithms (Deutsch–Jozsa [12], QFT [13], Grover [14] and Shor [15, 16]) were made. However, in none of them the size of the problem (in terms of qubits involved) was big enough to provide a real speed-up with respect to a classical computer.

In 2000, David P. DiVincenzo set five (plus two) reasonable criteria that a physical

implementation of quantum computer should satisfy [17]. These are:

- a scalable physical system with well characterized qubits

- the ability to initialize the state of the qubits to a simple fiducial state

- long relevant decoherence times, much longer than the gate operation time

- a "universal" set of quantum gates

- a qubit-specific measurement capability

The two additional criteria are given for a quantum computer capable of quantum communication:

- the ability to interconvert stationary and flying qubits

- the ability to faithfully transmit flying qubits between specified locations

From all of the proposed physical implementations of a quantum computer, the one which meets most of the requirements is the use of trapped ions [18]. However, like all the other implementations, scalability is still an outstanding challenge: to be of any practical use, a quantum computer must be able to store and process thousands of qubits [19], while the actual state of the art is of order of ten qubits [20].

One proposed way to scale-up the number of qubits in a trapped-ion quantum computer is the use of a multiplexed array of small traps, with segmented DC electrodes used to shuttle ions from the memory region to the processing region [21, 22]. Even if ion trapping was originally achieved by means of 3-dimensional quadrupole Paul traps, it seems that a reasonable way to build these arrays of traps is using planar surface traps [23]. Planar traps can benefit from photolithographic techniques to achieve miniaturization to sub-micrometer feature sizes, and several investigations were already done in this direction. Shrinking down the trap dimensions, the ion-electrodes distance is inevitably reduced. An unexpected technical challenge arose from this aspect is the *anomalous heating*: an increasing of the ion heating, due to electrical field noise, roughly proportional to d^{-4} (d being the ion-electrode distance). Since this effect is proven to be thermally activated, it can be reduced by several order of magnitude with the use of a cryostat [24].

Despite a lot of efforts spent in the miniaturization of ion-traps, not very much was done on the trap-drive electronics. In particular, the voltages necessary for the trapping are usually provided by means of bulky helical resonators [25], fed with several watts of input RF power. These amplifier are not ideal if the trap has to be operated in a small

cryogenic environment, like in the case of the "Cryotrap" experiment being developed at the University of Innsbruck. The goal of this thesis — as part of the Cryotrap experiment — is thus the investigation and the realization of a miniaturized, lumped components, passive voltage amplifier, with a voltage gain high enough to permit trapping with only few hundreds of milliwatts of RF power.

This thesis is structured as follows: chapter 2 describes the working principles of ion-traps and the constraints that the drive electronics should fulfill. Chapter 3 explains the underlying theory of RLC resonators and how to optimize both the components selection and the circuit design. The experimental apparatus is described in chapter 4, together with the experimental results of every built resonator. Finally, chapter 5 gives some suggestions about how to improve the actual setup.

2. Resonator requirements

As stated in the introduction, trapped ions are a suitable choice for the realization of a Quantum Information Processing (QIP) apparatus. In the first part of this chapter, Sec. 2.1, the fundamentals of ion trapping are summarized. The physics of trapping, along with a number of technical considerations, place constraints on the requirements for the driving electronics. These will be outlined in Sec. 2.2. Sec. 2.3 describes a number of possible resonators, and evaluates them against the constraints given. Finally, Sec. 2.4 introduces and gives some considerations for a matching network, which is needed to bind correctly a source and a load providing the maximum power transfer.

2.1. Ion-trap fundamentals

2.1.1. Trapping potentials

Trapping of charged particles has been extensively covered in the literature [26, 27]. The salient points are briefly reviewed here.

In general a particle is said to be trapped if it experiences a restoring force when it moves away from a specific point. The easiest example of such a force is the force applied by an ideal massless spring with an unloaded length of zero, connecting the particle and the trapping point. In this case the force is conservative and the related energy potential is harmonic and isotropic. More generally, in the case of an anisotropic harmonic restoring force, the energy potential looks like

$$U(x,y,z) = \frac{1}{2}(\alpha x^2 + \beta y^2 + \gamma z^2) \ . \tag{2.1.1}$$

When dealing with charged particles, one can build a specific energy potential just acting on the electric potential. In order to achieve the same as in Eq. 2.1.1, an electric potential of the form

$$\Phi(x,y,z) = \frac{U(x,y,z)}{Q} = \frac{1}{2Q}(\alpha x^2 + \beta y^2 + \gamma z^2) \tag{2.1.2}$$

must be prepared. Here Q is the particle's electrical charge. In free space, the Laplace equation holds. This imposes

$$\Delta U = \alpha + \beta + \gamma = 0 \ . \tag{2.1.3}$$

This, in turn, means that at least one of this coefficients has to be negative. The potential presents a saddle point instead of a minimum, causing an anti-trapping force in at least

one direction (as through a repelling spring). It is therefore not possible to trap in 3D using only static electric fields.

One possible bypass to this problem is to use radio-frequency electric potentials: the ion always feels a saddle-like potential, but the anti-trapping direction is changed periodically. For this reason the ion will move with two superimposed motions: a fast and small (in amplitude) oscillation, driven by the fast RF field, on top of a slower but bigger motion, driven by the field inhomogeneities. The first is called *micromotion* and the second is called *secular motion* (see Sec. 2.1.3 for details). The averaged force experienced by the particle can, under certain conditions (see Sec. 2.1.3), be trapping in all directions and for every sign of the electrical charge. In particular, this time-averaged force is conservative and can be expressed in terms of an electrical *pseudopotential* [28]

$$\Psi(x, y, z) = \frac{Q}{4M\Omega^2} |\nabla \Phi(x, y, z)|^2 \tag{2.1.4}$$

where M is the mass of the particle and Ω is the angular frequency of the applied RF field. Remembering that the electric field is $E(x, y, z) = -\nabla \Phi(x, y, z)$, it is straightforward to note that the potential increases with the square of the magnitude of the electric field. This means that the trapping point - i.e. the minimum of the potential - will coincide with the field node. Around this point, the energy potential $U_p = Q\Psi$ can be approximated to the lowest order with an harmonic potential. With this approximation it is possible to find the associated elastic constants, and from them the oscillation frequencies, called *secular frequencies*, simply using

$$\omega_i = \sqrt{\frac{k_i}{M}} \ . \tag{2.1.5}$$

Here the subscript i is used to indicate the principal trapping axis, found during the harmonic approximation. In general, the harmonic fitting can be different for the three axes, and the frequencies will be different, too. Since k_i is found from the fitting of Eq. 2.1.4, it is inversely proportional to the particle's mass. Thus, the overall dependency of the secular frequency to the mass is

$$\omega \propto \frac{1}{M} \ . \tag{2.1.6}$$

2.1.2. Ideal trap geometry

For simplicity, this section focuses only on *linear quadrupole traps*, but what follows can be extended easily to different geometries or even to multipole potentials [29]. A linear
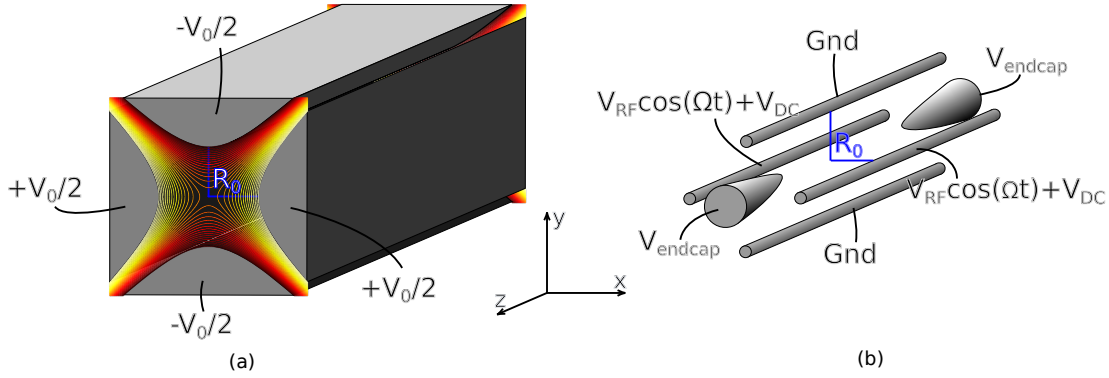
Figure 2.1: (a) The ideal Paul trap: four hyperbolically shaped electrodes, with a potential difference of V_0 between every pair of neighboring electrodes. Some isopotential lines are also shown. (b) A more general and practical configuration, with non ideal electrode's shape and two electrodes held to ground. Two endcaps are added to achieve axial confinement.

quadrupole trap (Paul trap [26]) is an electrode configuration such that the electric potential can be described with

$$\Phi(x, y, z) = \frac{1}{2}V_0 \left[\left(\frac{x}{R_0} \right)^2 - \left(\frac{y}{R_0} \right)^2 \right] . \tag{2.1.7}$$

The potential is like Eq. 2.1.2 with $\alpha = -\beta = QV_0/R_0{}^2$, $\gamma = 0$. It is possible to obtain this potential with four hyperbolically shaped rods, separated from the origin by R_0, and by applying opposite voltages $\pm V_0/2$ on adjacent electrodes (Fig. 2.1). A positively-charged ion in such a trap will not feel any force along z, an elastic force along x and an anti-elastic force along y. By applying an RF voltage, trapping can be achieved as explained above. In practice, rather than applying $\pm V_0/2$ on each electrode, it is much easier to hold two opposite electrodes to ground and applying

$$V(t) = V_{\text{RF}} \cos(\Omega t) \tag{2.1.8}$$

to the others. In this way only one RF signal is needed and the relevant physics is unchanged because the field lines are exactly the same as before.
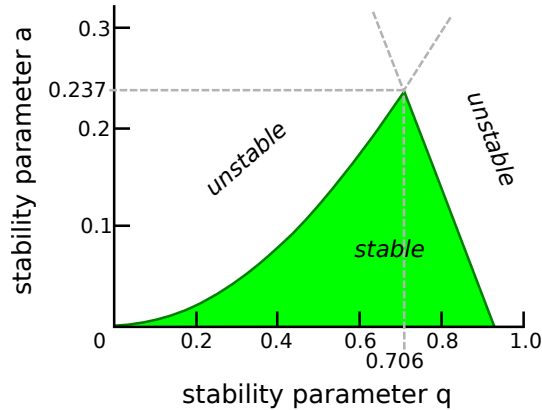
Figure 2.2: Stability diagram for a linear quadrupole trap. Both axes are symmetrical with respect to the origin. This diagram can be found in [26].

2.1.3. Trapping stability

In the particular case of a quadrupole RF trap, the equations of motion for the charged particle (in our case, an ion) take a simple form which can be analytically solved [26]. For the linear trap described above, and applying both an RF and a DC potential to the electrodes, as shown in Fig. 2.1 (b), these are

$$\ddot{x} = -\frac{Q}{MR_0{}^2}\left[V_{DC} + V_{RF}\cos(\Omega t)\right]x \qquad (2.1.9)$$

$$\ddot{y} = \frac{Q}{MR_0{}^2}\left[V_{DC} + V_{RF}\cos(\Omega t)\right]y \qquad (2.1.10)$$

where V_{RF} is the amplitude of the applied radio frequency voltage and V_{DC} is the value of the applied static electric potential. The above differential equations are a special case of the well known Mathieu equations, where the stability parameters a and q are

$$a = \frac{4QV_{DC}}{MR_0{}^2\Omega^2} \qquad q = \frac{2QV_{RF}}{MR_0{}^2\Omega^2} \; . \qquad (2.1.11)$$

"Stability", here, means that the ion trajectories are bounded when the trap is operated with such a and q parameters. Different regions of stability exist in the (q, a) parameter space. The most important one (for practical purposes) is the one at the lowest a. A plot of this region can be seen in Fig. 2.2. For $a << 1$ and $q^2 << 2$ the ion's trajectory has an analytical form:

$$x(t) = x_0 \cos(\omega t + \varphi)\left[1 + \frac{q}{2}\cos(\Omega t)\right] \qquad (2.1.12)$$
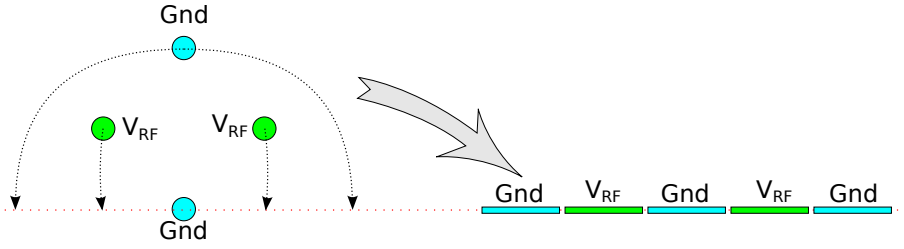
Figure 2.3: Planar surface traps are linear traps where the electrode configuration has been deformed such that the electrodes lie on the same plane.

and similarly for y, where x_0, and φ depend on the initial conditions and where

$$\omega = \frac{\Omega}{2}\sqrt{a + \frac{1}{2}q^2} \qquad (2.1.13)$$

is called the secular frequency and coincides with the one mentioned above. Now we can see in a rigorous way that the motion has two contributions:

- a fast *micromotion* at the RF frequency

- a slower *secular motion* at the secular frequency

When the length of the trap in the z direction (trap axis) is much bigger than the other two directions, the RF contribution to the axial motion can be neglected. Thus, no micromotion is present along the trap axis, in first approximation.

2.1.4. Non-ideal traps

Linear Paul traps have been used in a huge variety of applications, from mass spectroscopy to quantum information [26, 30, 31]. For the long-term goal of building a quantum computer these traps seem not to be the optimal choice because of the intrinsic difficulties in scaling such a system [32]. One appealing and promising kind of trap is the planar surface trap. In these traps the electrode configuration has been deformed such that the electrodes lie on the same plane (Fig. 2.3). The most evident advantages of this are:

- wider optical access (half solid angle)

- use of photolitography for the fabrication, which leads to:

- scalability to micrometer dimensions

- easier implementation thanks to standard industrial fabrication techniques

Of course, these traps will present different potentials, which in general will be non-harmonic. However, the remarkable result is that - on axis, near the field node - the physics remains exactly the same as before, except for a dimensionless geometry factor $\eta \lesssim 1$. In traps which do not have a perfect harmonic potential, all the calculations done so far are valid only within this approximation. Noting that Eq. 2.1.4 is completely general - i.e. it does not require $\Phi(x, y, z)$ to be harmonic - it is possible to calculate numerically the pseudopotential, using some finite element software like COMSOL Multiphysics®, and then check how good the harmonic approximation is, near the trapping field node. Writing the RF potential as

$$\Phi(x, y, z, t) = V_{\mathrm{RF}}\phi(x, y, z) \cos\left(\Omega t\right) \tag{2.1.14}$$

it is easy to see that the normalized time-independent part - $\phi(x, y, z)$ - is the only thing needed to be simulated. From this, the pseudopotential can be calculated and fitted with a parabolic potential. Using the fitting constants and Eq. 2.1.5, it is possible to estimate the secular frequencies in all the principal axis. The calculation yields

$$\omega_i = \frac{QV_{RF}}{\sqrt{2}M\Omega}\sqrt{\frac{\partial_{x_i}^2 \left|\nabla\phi(x, y, z)\right|^2}{2}} \tag{2.1.15}$$

where the partial derivative is taken along the principal axis x_i at the trap center. Equating the calculated secular frequency with the ideal one (Eq. 2.1.13), it is possible to find the geometric factor stated above. This is

$$\eta = R_0'\sqrt{\frac{\partial_{x_i}^2 \left|\nabla\phi(\mathbf{r})\right|^2}{2}} \tag{2.1.16}$$

(R_0' being the shortest ion-electrode distance).

An example of a non-ideal trap is *Yedikule-1*, the first surface trap — drawn by N. Daniilidis and M. Niedermayr in 2008 — built in our cleanroom. In Fig. 2.4, a top-view schematic of this trap can be seen. Orange-colored electrodes are held at ground, the green-colored electrode is the RF one and the blue-colored electrodes are held at independent DC voltages. Ions are trapped along the RF null, $454\,\mu$m above the trap surface. Note that an ion sitting at the trap center sees, in the xy plane, two RF rails, exactly like in the quadrupole trap, but three DC electrodes. This does not change the
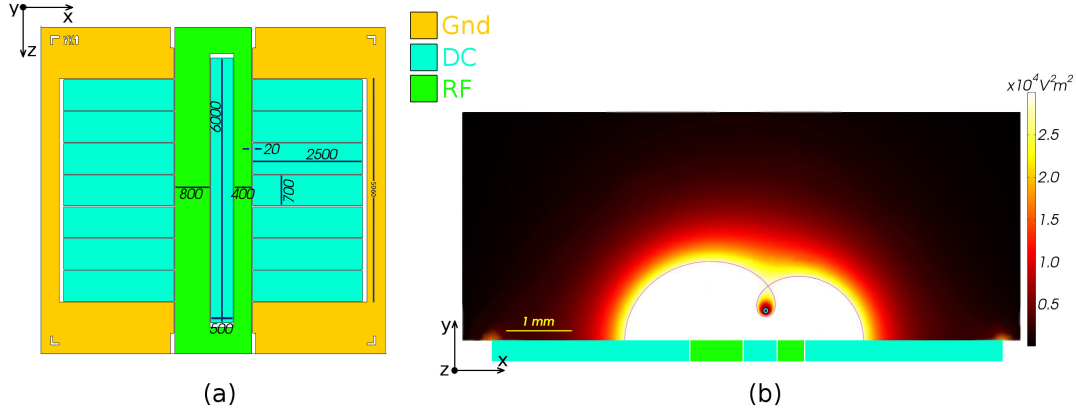
Figure 2.4: Our first planar surface trap Yedikule-1. (a) Top view of the trap, with dimensions in microns. (b) Numerically simulated 2D normalized pseudopotential, in the xy plane crossing the center of the trap. The electrodes' thickness is artificially increased here just to show them better.

idea behind the quadrupole trap, and allows for more freedom in shaping the electrical potential around the trapping center, giving the ability to compensate for unwanted stray fields. Also note that applying a voltage of $\sim 25\,\mathrm{V}$ to the four outermost DC electrodes, axial confinement can be achieved, too, as in the case of the endcap electrodes in Fig. 2.1 (b). The normalized pseudopotential, $|\nabla\phi(x,y,z)|^2$, was simulated using COMSOL and it is reported in Fig. 2.4 (b). From the fitting done in this region all the trap parameters were calculated. These are reported in Tab. 1. Finally, note that the principal axes are rotated with respect to the spatial ones. This means that a cooling laser, coming parallel to the surface, can cool all the directions at the same time.

2.2. Desiderata

As shown above, ion traps must be driven with a radio frequency voltage source. A lot of effort was spent in the last years to find suitable ways to scale down traps, but almost nothing was done for scaling or improving the driving electronics. This thesis is all about my attempts to do so. In particular, this section will explain the constraints given by the physics, the dimensions and the trap stability to the driving electronics.

The common choice for the stability parameter a is 0, which means no DC offset on the RF electrode, while for the stability parameter q values between 0.4 and 0.7 are usually chosen. These values for q provide robust trapping even in presence of small

Parameter	Symbol	Value	Unit
RF stability parameter	q	0.6	
RF drive frequency	$\Omega/2\pi$	10	MHz
RF voltage amplitude	V_{RF}	365	V
Secular frequency	$\omega_{\mathrm{x}}/2\pi$	2.08	MHz
	$\omega_{\mathrm{y}}/2\pi$	2.166	MHz
Trapping well depth	ΔE	0.58	eV
Trapping height	R_0	454	μm
Trap efficency	η_{x}	0.27	
	η_{y}	0.28	
Principal axis rotation	θ_{T}	5	°
Trapping region dimensions	$W \times H$	300×400	μm^2
Capacitance	C_{trap}	1	pF

Table 1: Example of simulated Yedikule-1 parameters. The imposed parameter q and Ω where chosen for stability and practical reasons. From these and the geometrical constraints, all the other parameters where calculated. Note that these numbers are shown here for demonstration purposes only, and can be different for the final resonator.
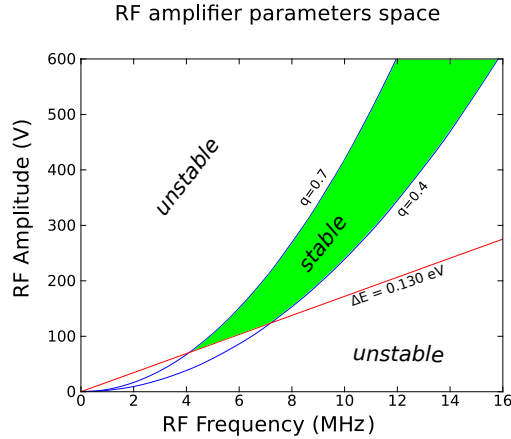
RF amplifier parameters space

Figure 2.5: Stable ion trapping can be robustly performed if the RF amplitude and the frequency are chosen to provide $0.4 < q < 0.7$ and $\Delta E > 0.130\,\mathrm{eV}$. In the green region these constraints are fulfilled for Yedikule-1.

residual DC stray fields. When these fields are properly compensated, lower values ($q \sim 0.2$) can be used, too. Requesting also for a minimum well depth of $\Delta E = 0.130\,\mathrm{eV}$, which is equivalent for the kinetic energy of a particle at $1000\,\mathrm{K}$ (the atomic source of $^{40}\mathrm{Ca}$ starts to emit at a significant rate at $700\,\mathrm{K}$), one can calculate the range of possible RF amplitude and frequencies. This range of parameters is plotted in Fig. 2.5, for the particular case of Yedikule-1. As can be seen, the frequency should be chosen higher than $\sim 7\mathrm{MHz}$ to fulfill the well-depth constraint.

High voltages should be avoided for three reasons:

- to prevent arcing between the electrodes. This effect is studied in [33], and a specific application to planar traps can be found in [34]. Unfortunately, the upper voltage limit before breakdown strongly depends on the electrode's roughness. An estimation of this limit, for a gold trap on a quartz substrate, with an electrode separation of $20\,\mu\mathrm{m}$, is $\sim 600\,\mathrm{V}$.

- the difficulty in getting such high voltages on the trap's electrodes. The trap is mounted in the inner shield of a $4\,\mathrm{K}$, Gifford-McMahon type, cryostat. Cables have to be thermalized from $300\,\mathrm{K}$ to $4\,\mathrm{K}$ by means of conductive dissipation with the cold copper of the cryohead, and to do so cable at least as long as $\sim 0.5\,\mathrm{m}$, with a low thermal conductivity, have to be used. Unfortunately, low heat conductivity also means low electrical conductivity and this, in turn, means high Joule dissi-

pation. In our case we used two different coaxial cables, with the first one made of steel, and giving a total resistance of about $16\,\Omega$. If the full RF amplitude (of $\sim 100\,\mathrm{V}$) were directly applied to the trap via these cables, the power dissipated would be at least $32\,\mathrm{W}$ (considering also an impedance matching, see Sec. 2.4). This heating would be definitely too much to be properly cooled by the cryohead, which has a declared cooling power of $500\,\mathrm{mW}$ at $4\,\mathrm{K}$. The trap itself does not dissipate electric power because, at least in the ideal case, it behaves just as a capacitor. The only reasonable way is, then, to keep the RF signal the smallest possible during all the path toward the trap and only later amplify it, as close as possible to the electrodes.

- the difficulty in generating high voltages inside the cryostat. High voltages can be reached by means of active or passive voltage amplifiers. A plethora of active amplifiers does exist, but all of them are based on semiconductor technology, which does not perform at cryogenic temperatures. Passive amplifiers have quite poor performances (in terms of voltage gain) when compared to the active ones, but they can work at low temperatures. Driving one of these amplifiers with a function generator, whose maximum transferred power is $250\,\mathrm{mW}$ ($5\,\mathrm{V}$ amplitude), and requiring an amplified RF amplitude bigger than $100\,\mathrm{V}$, an overall voltage gain of at least 20 is needed.

Another important requirements to be fulfilled by the amplifier is that the amplifier has to be vacuum compatible. During the prototyping of the amplifier, only little care was taken for that problem. The reason is that our amplifier was going to operate at cryogenic temperatures, where outgassing is not a problem anymore. Every electronic component should be tested (very little information about vacuum compatibility is specified in datasheets), as well as solder and printed circuit board (PCB) material. For the latter a very common choice is Rogers RO3003 [35].

Similarly, cryogenic compatibility is an important aspect which is not easy to control. Datasheets usually report temperature coefficients down to $-50\,°\mathrm{C}$, and the only way to prove compatibility is to test every single piece. Most of the components we tested worked at low temperature with small and reproducible variations. The biggest problem that we encountered was the instability of the connections, especially in coaxial connectors, at low temperature.

The final constraint is the physical dimension. The inner shielding in our cryostat, where the trap lies, is $10\,\mathrm{cm}$ in diameter, and most of the space is used for the trap holder, the activated charcoal pump and the wiring (Fig. 2.6). The maximum room left for the amplifier is not bigger than few cubic centimeters.
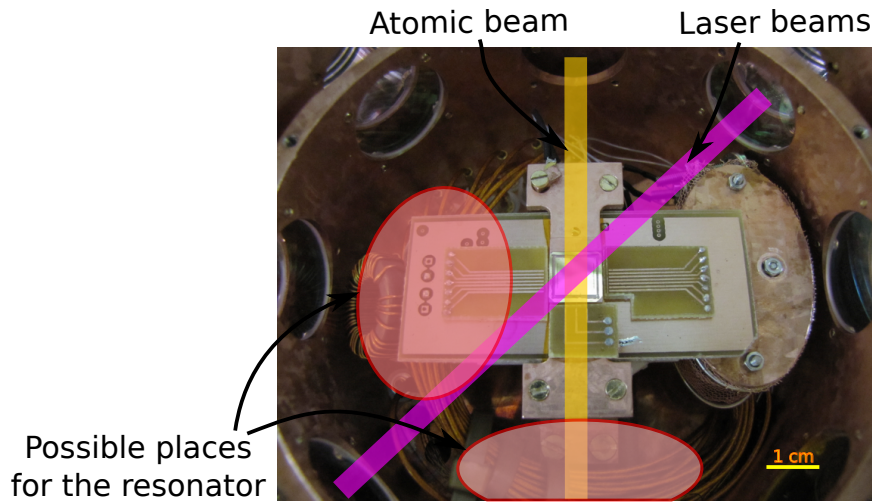
Figure 2.6: Inside of the cryostat. There are two suitable places for the resonator, each of no more than $\sim 10\,\mathrm{cm}^3$.

Summarizing, the constraints in the RF amplifier design for our trap and our cryostat are the following:

- RF drive frequency $\Omega/2\pi > 7\,\mathrm{MHz}$

- Voltage gain $G_V > 20$

- Vacuum compatible

- Cryogenic-temperature compatible

- Smaller than $10\,\mathrm{cm}^3$

All of them can be fulfilled by a passive electronic resonator.

2.3. Types of resonators

As shown above, the natural choice for applying a high RF voltage across the trap electrodes is the use of an electronic resonator. These devices are the counterparts for mechanical resonators, like pendulums, where a small resonant force can drive high amplitude oscillations in the system. This can happen only if the power dissipated by the system is less then the power transferred to it, when the oscillation amplitude is
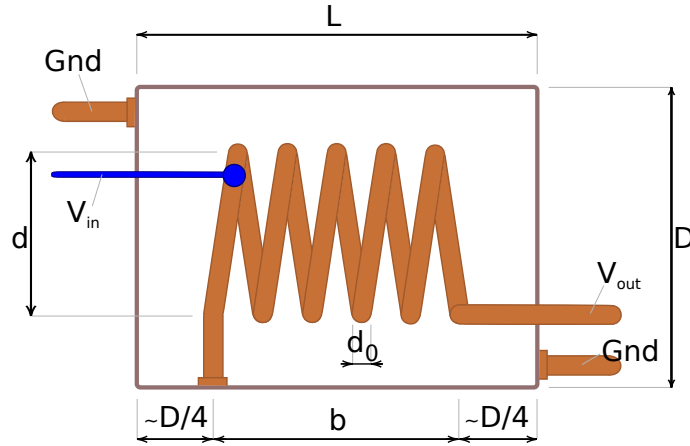
Figure 2.7: Diagram of a quarter-wavelength helical resonator.

small. The excess of energy is stored in the form of both potential and kinetic energy, and grows until the dissipations are equal to the incoming power. As long as the stored energy increases, the oscillation amplitude increases accordingly.

There are three types of resonators working in the frequency range we are interested in: helical, RLC and crystal oscillators [36, 37]. For the first two types of resonators the energy is stored in the electric and magnetic field produced by the the simultaneous presence of an inductive and a capacitive load. Both of them operate essentially in the same way, though an helical resonator is a distributed component circuit while an RLC circuit uses lumped components. The High Frequency (HF) radio frequency band, which extends from 3 to 30MHz and covers the region of our interest, is basically a cross-over band. Here frequencies are too high to have good lumped components, and at the same time the electric wavelengths are too long to have high quality, small sized distributed component. Both helical and RLC resonators can be used to amplify a voltage, but till now only helical resonators were typically used to drive ion traps [38]. Unfortunately none of the two is the perfect solution for every application. Here I will try to introduce them briefly and to mark their respective advantages and disadvantages.

2.3.1. Helical resonator

Helical resonators are a special kind of coaxial quarter-wavelength resonators, where the central conductor is wound as a single-layer solenoid, or helix, and is electrically connected to a surrounding conducting shield (Fig. 2.7). They are usually meant for

higher frequencies (Very High – VHF – and Ultra High – UHF – frequencies bands), since their physical dimensions are dependent on the wavelength which, for HF, ranges from 10 to 100 m in free space. Since the resonator acts as a waveguide, it is possible to change the phase velocity of the electromagnetic wave (and hence the wavelength) by changing the distributed capacitance ($\mathcal{C}$) and inductance ($\mathcal{L}$). The resonant condition to satisfy is

$$b = \frac{\lambda}{4} = \frac{v}{4\nu} = \frac{1}{4\nu\sqrt{\mathcal{L}\mathcal{C}}} \tag{2.3.1}$$

where λ and v are the wavelength and the phase velocity in the medium, while $\nu = \Omega/2\pi$. The formulae for $\mathcal{C}$ and $\mathcal{L}$ as a function of the ratio d/D (see Fig. 2.7) can be found in [25, 37]. The unloaded quality factor Q_{H} (more detail in Sec. 3.1.1), which is related to the maximum voltage gain achievable, is also a function of the sizes of the resonator. In the usual case of a copper helical resonator, with a non magnetic shield, and where the optimal parameters $d/D = 0.55$ and $b/d = 1.5$ are used, the quality factor is

$$Q_{\mathrm{H}} = 1.97 D\sqrt{\nu} \, /\mathrm{m}\sqrt{\mathrm{Hz}} \, . \tag{2.3.2}$$

In our case, where an important and stringent constraint is the size, D cannot be chosen to be bigger than 1.4 cm, in order to remain with a total volume below $\sim 10\,\mathrm{cm}^3$ (optimum $L = 1.8\,\mathrm{cm}$). With this diameter the highest Q_{H} which can be obtained is 78 at 8 MHz.

Helical resonators are the common choice for other ion traps, which are operated at higher frequencies and at room temperature. The latter means that the amplifier can be put just outside the chamber and then connected to the trap with two short wires and this, in turn, means that the resonator has much less stringent size limits. With bigger resonators very high quality factors can be achieved, as high as several thousand (Fig. 2.8). However, in the perspective of a scalable technology for trapped ion quantum computing, sizes matter, and small helical resonators have poor performances. Another drawback of helical resonators is that building them small becomes more and more difficult. As an example, the wire diameter should be half the winding pitch in order to get the best Q_{H}. This, always in the perfect case, leads to

$$d_0 = \frac{8.55 \cdot 10^{-9}}{\mathrm{m} \cdot \mathrm{Hz}} \cdot D^2\nu \tag{2.3.3}$$

where d_0 is the wire diameter. For a 1.4 cm resonator operating at 8 MHz, the wire diameter should be a little bit more than 0.01 mm. The number of windings becomes extremely high, too, with more than 430 turns. In addition, the tapping point - i.e. the place where the cable with the incoming signal is soldered to the helix - must be found
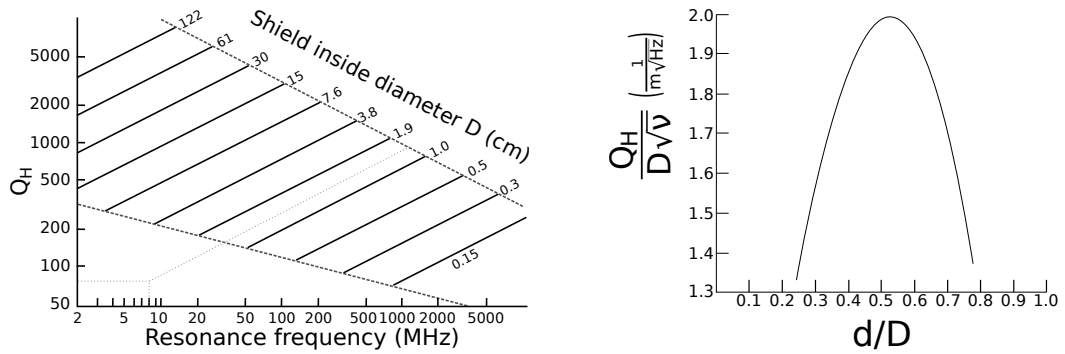
Figure 2.8: Unloaded quality factor Q_{H} for an helical resonator, *(left)* as a function of the shield diameter D and the resonant frequency ν and *(right)* as a function of the ratio d/D [25, 37]. The blue lines in the first plot indicate the region where, usually, it is preferred to use a helical resonator instead of other resonators.

by trial and error. A wrong tapping point leads to reflections in the traveling waves and decreases the total gain. With such a small wire the search for the proper tapping point becomes challenging. Finally, the proper ratio d/D is of great importance to get the highest Q, and this can be a technical problem during the construction of the resonator. As can be seen in Fig. 2.8, the quality factor quickly decreases if the ratio d/D changes from the optimal parameter 0.55. All these reasons (tapping, imperfect machining and structural problems) are limiting factors for the expected Q_{H}. Helical resonators are therefore not a scalable solution, at least not for small drive frequencies.

2.3.2. Series RLC resonator

Since a distributed component circuit cannot be efficiently scaled down, an alternative is to use lumped-component circuits. The archetype for a lumped-component resonator is the series RLC circuit (Fig. 2.9), where the inductor and the capacitor are the reactive components which will store the energy, while the resistance is an equivalent resistance which is due to dissipation through wires, components and even emitted radiation. Viewing the circuit as a voltage divider, one can see that at low frequencies the voltage transfer has a gain of 1, while at high frequencies the gain is 0. However, at an intermediate frequency, the voltage gain across the plates of the capacitor is maximum
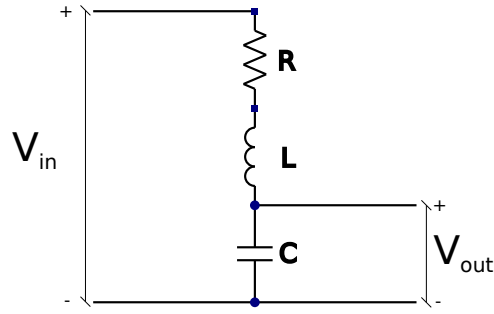
Figure 2.9: Resonant series RLC circuit, shown explicitly as a voltage divider.

and equal to

$$G_V = \frac{|V_{out}^{\max}|}{|V_{in}|} = \frac{1}{R}\sqrt{\frac{L}{C}} = Q \ . \tag{2.3.4}$$

The frequency at which the voltage gain is maximum is called *resonant (angular) fre-quency* and is given by

$$\omega_0 = \frac{1}{\sqrt{LC}} \tag{2.3.5}$$

when R is negligible. It is possible - and useful - to rewrite G_V in terms of the resonant frequency

$$G_V = Q = \frac{\omega_0 L}{R} \ . \tag{2.3.6}$$

The capacitive load C is given by the capacitance of the trap itself, plus that of any additional capacitors. In order to increase the voltage gain, it is easy to see from Eq. 2.3.4 that this extra capacitance should be kept as small as possible. Since the voltage gain is linear with the resonant frequency, while the required voltage to reach a specified trap stability parameter q increases quadratically, some overload can be added to the resonator to lower the resonant frequency, when this is too high. Moreover, it is important to say that the effective R is almost entirely given by the real winding resistance of the inductor's coil, which is linear with L (for a given wire material and diameter). Thus, most of the efforts must be used to try different kind of inductors: different materials, different cores, or different wire diameters, always aiming to find the best quality factor, which is the ratio between reactance and resistance

$$Q_L(\omega) = \frac{\omega L}{R} \ . \tag{2.3.7}$$

At resonance the relation $Q_L(\omega_0) = Q$ holds, because we attributed the R totally to the inductor.

2.3.3. Parallel RLC resonator

A parallel RLC resonator, sometimes also called "tank" resonator, is the dual circuit of the series circuit explained above. The resonance frequency is again given by Eq. 2.3.5, but this time the gain is for the current and not for the voltage. The gain is given by

$$G_I = \frac{I_C}{I_{in}} = \frac{R}{\omega_0 L} = \omega_0 R C \qquad (2.3.8)$$

which is also the quality factor. Note that R, in this case, is meant to be very high, as opposed to the series case where it was small. It is still used to model the circuit dissipations, but, especially in this parallel form, it can be seen as a "leak". It takes into account for leaks through the capacitor's dielectric or the parasitic currents in the inductor's core. On resonance the impedance is at its maximum, and is equal to R. Since the voltage across each component is equal to the voltage applied from the outside to the circuit, it may seem that this circuit can not be used as a voltage amplifier. This is not completely true. If a matching network is set at its input, the high impedance of the resonator forces the matching to increase the voltage (see Sec. 2.4 for detail). The complete matched resonator can, thus, be used as a voltage amplifier. As expected, using the same L and the same C to build a series or a parallel resonator, both with a matching circuit at the input, leads to the exact same voltage gain at the same resonant frequency.

2.3.4. Crystal oscillators

In contrast to the first three resonators, in crystal oscillators the accumulated energy is stored in the electric field, in the kinetic (vibrational) energy and in the elastic potential energy. Thanks to the piezoelectric property of these crystals, oscillations on the surface of the material are transduced to and from oscillating electric field. Stimulating a crystal with a sinusoidal voltage, higher and higher oscillation amplitudes are formed.

The vibrational modes are constrained by the physical dimensions of the crystal, so these devices always have a very pure excitation spectrum, with a sharp peak across the resonance frequency. For this reason they would be the ideal choice to drive an ion trap and at the same time filtering the RF voltage from unwanted noise. This is important because electric noise at the ion's secular frequencies will transfer energy to the ion itself, leading to heating and quantum decoherence. Unfortunately these resonators have insurmountable disadvantages:
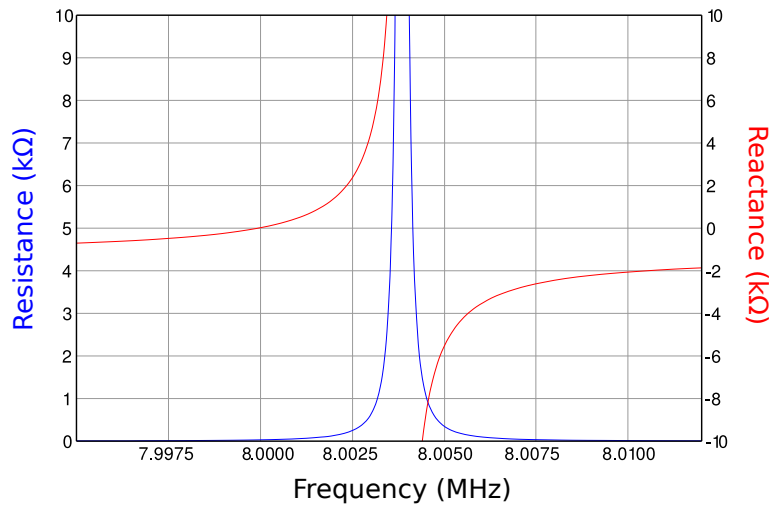
Figure 2.10: Crystal's impedance near resonance. The natural (series) resonance is at 8.00MHz.

- their tunable range is very small

- they do not support high power

- in order to get a high oscillating electric potential, it is possible to stimulate the crystal either mechanically (directly) or using another electric field. The first case is difficult since the mechanical stimulus has to be at RF frequency. The second case is difficult because of the necessity to couple and uncouple the oscillator during the swinging, like in the case of a pendulum.

For these reasons a quartz oscillator is not a suitable voltage amplifier but, if tunability is not necessary, one can exploit their performance as a frequency selector for filtering unwanted noise.

Another interesting feature is the crystal's impedance. This changes very sharply with frequency in the region near resonance, and presents inductive or capacitive behavior just slightly detuning above or below resonance (see Fig. 2.10). Using a crystal as part of a matching network can thus exploit this feature. The only limitation is given by the low power they can support.

2.3.5. Resonator choice

In the range of frequencies of our interest, three types of resonators are available but none of them is completely superior to the others. In the presentation done so far, the advantages and disadvantages were pointed out. Helical resonators have good quality factors, but are limited when scaled down and are difficult to build. Crystal oscillators have excellent quality factors, are small, but cannot be tuned and cannot easily used to amplify a voltage. RLC circuits have quality factors which are limited by the quality of the components, especially the inductor, but are easy to build, quite reproducible and small. Given these considerations, the RLC resonator was our last decision.

2.4. Matching network

It was noticed previously that a matching network is necessary to achieve a voltage gain with a parallel resonator. However, a matching circuit is much more than this. Its goal is to eliminate any possible reflected power from a load when this is attached to a source. This is necessary for at least three important reasons:

- prevent waste of power, and thus unnecessary dissipation. Working at low temperature, dissipation is a significant concern.

- Increase the voltage gain. Of course, if the power is completely transferred to the load the voltage gain is increased as well.

- Protect source's life. If a power amplifier is used as source, care must be taken to avoid reflections which could destroy the amplifier itself.

Power reflections happen when the source impedance Z_s is not equal to the complex conjugate of the load impedance Z_l^*. The goal of the matching is thus to transform a particular load to be equal to the (conjugate) impedance of the source. Modeling the matching circuit as a black box, it is possible to divide the circuit in two separate parts: an input and an output. The load impedance, seen from the source, is given by the ratio

$$Z_i = \frac{V_i}{I_i} \tag{2.4.1}$$

while the relation between current and voltage at the output is constrained by the real load impedance
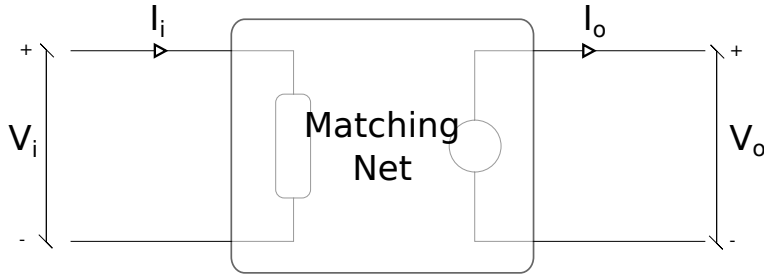
$$V_o = I_o Z_l \ . \tag{2.4.2}$$

Figure 2.11: A matching network is a generic "black-box" which can transform a load impedance to be equal to the complex conjugate of the source's output impedance.

If the black box is only composed of passive elements, and dissipations inside the box itself are ignored, the power conservation relation holds

$$|V_i I_i^*| = |V_o I_o^*| \, . \tag{2.4.3}$$

Let k^2 be the transformation ratio $|Z_l|/|Z_s|$. Using the above equations and remembering that the load is matched when $Z_i = Z_s^*$, it is easy to see that

$$k^2 = \frac{|V_o|^2}{|V_i|^2} \, . \tag{2.4.4}$$

This means that the voltage gain of a matching network is equal to k, and that the overall gain of a matched resonator is given by

$$G_V^M = k \frac{1}{R} \sqrt{\frac{L}{C}} = \sqrt{\frac{L}{|Z_s| RC}} \tag{2.4.5}$$

in the series RLC case. Improving the resonator's gain by reducing R has only a square-root effect on the complete circuit. Similarly, it is easy to see that the impedance of a parallel resonant circuit, which is usually very high, can be matched only using a matching network which increases the voltage.

In oder to build a matching network, it is first necessary to quantify the mismatch. Suppose that no matching block is inserted in the circuit, so that this is viewed as a generic load from the source. Calling V_i the incoming voltage applied to a load in the ideal case $Z_s = Z_l^*$, and calling V_t the total voltage applied to the load in the general case, it is possible to find the reflected voltage $V_r = V_t - V_i$. A scattering parameter S

can than be defined as the reflected voltage V_r, normalized to the incoming voltage V_i. From this definition, and with V_s being the source (internal) voltage

$$V_\mathrm{t} \;=\; V_\mathrm{s}\frac{Z_\mathrm{l}}{Z_\mathrm{l}+Z_\mathrm{s}} \tag{2.4.6}$$

$$S \;=\; \frac{V_\mathrm{r}}{V_\mathrm{i}} = \frac{V_\mathrm{s}\frac{Z_\mathrm{l}}{Z_\mathrm{l}+Z_\mathrm{s}}}{V_\mathrm{s}\frac{Z_\mathrm{s}^{*}}{Z_\mathrm{s}^{*}+Z_\mathrm{s}}} - 1 \tag{2.4.7}$$

$$\;=\; \frac{Z_\mathrm{l}Z_\mathrm{s} - Z_\mathrm{s}^{*}Z_\mathrm{s}}{Z_\mathrm{s}^{*}Z_\mathrm{l} + Z_\mathrm{s}^{*}Z_\mathrm{s}}\ . \tag{2.4.8}$$

In the special case where Z_s is real, typical for instrumentation and transmission lines, becomes

$$S = \frac{Z_\mathrm{l}-Z_\mathrm{s}}{Z_\mathrm{l}+Z_\mathrm{s}} = \frac{\mathcal{Z}-1}{\mathcal{Z}+1} \tag{2.4.9}$$

with $\mathcal{Z} = Z_\mathrm{l}/Z_\mathrm{s}$ being the normalized load impedance.

A common way to represent S is using polar coordinates on an Argand-Gauss complex plane. On the same plane, and using Eq. 2.4.9, it is possible to draw lines which link S and $\mathcal{Z}$. This figure is called the *Smith chart* (reported in Fig. 2.12), and it is a very useful tool for impedance matching. The chart can be used as a map, where every $\mathcal{Z}$ can be matched to $\mathcal{Z} = 1$ following the curves which correspond to parallel or series reactances. It should be noted that avoiding resistances is preferable because of dissipation.

As stated before, impedance matching is strictly related to voltage transformations. The most common way to achieve this is using transformers and voltage dividers. Both of these can, indeed, be used as a matching circuit. For transformers the relevant equation is given by Eq. 2.4.4. They are typically used in broadband matching, when the frequencies used are much lower then the self resonance of the transformer itself. Due to the difficulty to fine-tuning a transformer, other alternatives are preferable.

A voltage divider, commonly called an *L-section* for its topology (see Fig. 2.13), can also be used to increase or decrease a loading impedance. If the first reactance - viewing from the load side - is in parallel (Fig. 2.13 *(a)*), the total impedance is diminished. If the reactance is in series (Fig. 2.13 *(b)*) it is increased.

In Fig. 2.12 four different zones are marked. These correspond to specific zones for "L-section" matching:

Zone 1. The first component must be placed in parallel to the load.
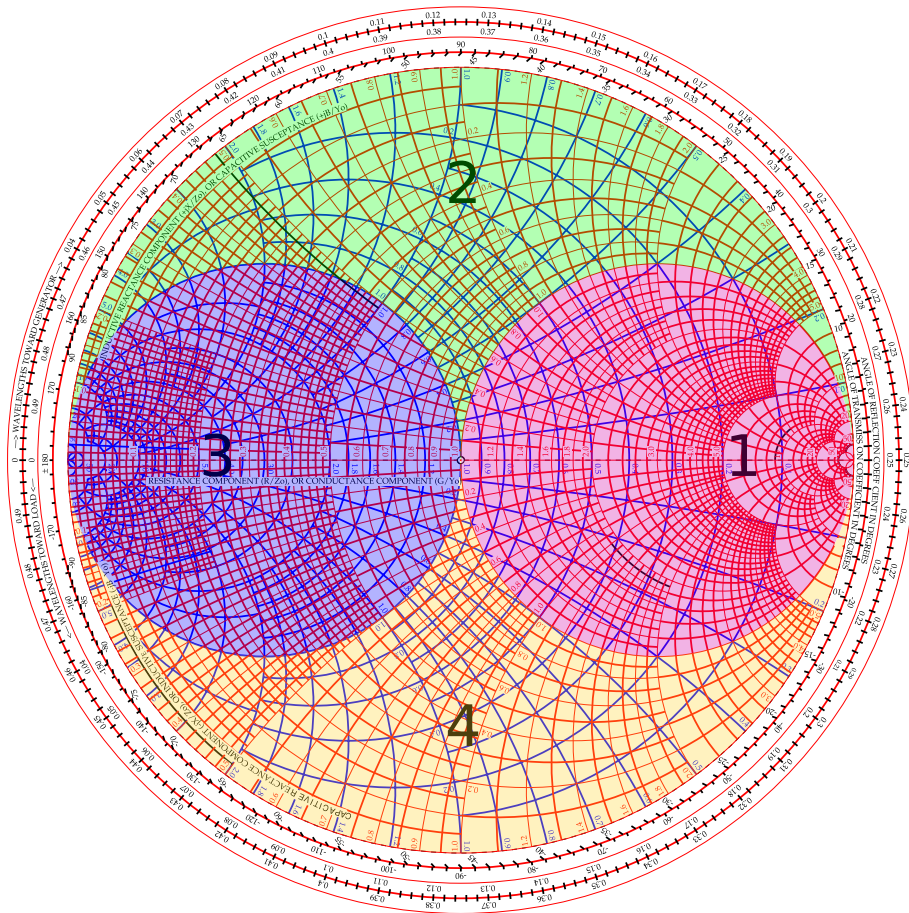
Zone 2. The first component must be a capacitor.

Figure 2.12: Smith charts are a useful way to represent impedances and admittances on the same plot, thus providing a map for impedance matching. Different regions correspond to different possible kinds of matching. The picture is a modified version of the Smith chart available at http://rfic.ucsd.edu/files/smith_chart.pdf (2011.06.01).
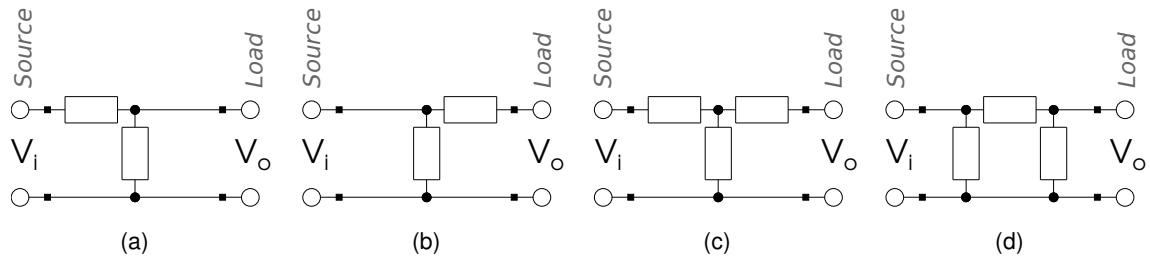
Figure 2.13: The four commonly used matching networks. *(a)* and *(b)* are called "L-sections", *(c)* is called "T-section" and *(d)* is called "PI-section". In *(a)* and *(d)* the first impedance, as seen from the load, is in parallel. In *(b)* and *(c)* the first impedance is in series.

Zone 3. The first component must be placed in series to the load.

Zone 4. The first component must be an inductor.

"PI" and "T" sections are just two cascaded "L" sections set back to back. They are used to increase or reduce the selectivity (reducing or increasing the bandwidth) of the match. Especially in filter synthesis, more than two cascaded "L" sections are used, where every single one just changes the voltage by a small step [39]. The advantages of doing so is to reduce the so called *insertion loss*. In the case of an ion trap, where the resonator should be operated at a single frequency and where the main losses are due to the resonator's inductor, a simple "L-section" is suitable.

2.5. Summary

This chapter presented an introduction to the RF amplifier and to its development. It explained the context in which this circuit should be used, followed by a discussion about the design constraints given by the specific application. Then the possible building blocks to be used were shown and carefully compared, in order to give a first, rough, choice. To optimize the features of the amplifier it is still necessary to look into the theory and to perform quantitative and optimal selection of the components. This will be discussed in the next chapter.

3. Designing a resonator

This chapter covers the design of the chosen RF amplifier, namely, an RLC amplifier. The design development starts from the RLC theory (Sec. 3.1), which is the basis for the components selection and optimization, explained in the following sections (Sec. 3.2 and Sec. 3.3). The topic of the final part (Sec. 3.4) is the development of a suitable PCB: the interfacing part connecting the resonator and the trap itself.

3.1. Theory

3.1.1. Resonator's quality factor

A critical parameter in discussing resonators is the quality factor Q. Its definition is not of very practical use when measuring, especially in the RLC case, but it is a very general definition and can be used to compare even different types of resonators, whether they are mechanical, electrical, optical, acoustic etc. The definition is

$$Q = \omega_0 \frac{E}{W} \tag{3.1.1}$$

where E is the energy stored in the resonator, and W is the averaged dissipated power. The importance of the definition became evident noting that Q is an estimation of how many cycles are needed to dissipate completely the stored energy and to stop oscillating. In the RLC case the stored energy transforms continuously from and to the electric and magnetic field. The maximum energy stored in the magnetic field - which is also the total energy stored in the resonator - is $E = 1/2\,LI^2$. The averaged dissipated power can be calculated with the Joule formula, which is $W = 1/2\,I^2R$ for a sinusoidal current of amplitude I. From these equations and the definition of Q, it is possible to write

$$Q = \frac{\omega_0 L}{R} = \frac{1}{\omega_0 RC} \tag{3.1.2}$$

where the resonance frequency ω_0 was already defined in Eq. 2.3.5.

3.1.2. Unmatched resonator

Series and parallel RLC resonators can be used as voltage amplifiers. The key-point of these circuits is the energy storage due to the simultaneous presence of an inductor and a capacitor. These components are never ideal and some dissipations always occur in the resistance of the coil and the wires, as well as in the parasitic currents in the capacitor's

dielectric. For this reason the Ohmic resistance cannot be omitted in the circuit analysis. As stated previously, any amplifier should be matched as well as possible to the source impedance. However, in order to find how the relevant parameters - i.e. Q and ω_0 - influence the RLC resonator alone, in this first calculation the matching network will be omitted.

The complex impedance of a series resonator, like the one in Fig. 2.9, is given by

$$Z(\omega) = R + i\omega L - \frac{i}{\omega C} = R\left[1 + iQ\left(\frac{\omega}{\omega_0} - \frac{\omega_0}{\omega}\right)\right] . \tag{3.1.3}$$

On resonance the impedance is at its minimum and it is equal to R. The reactance of the capacitor and the inductor cancel each other and the impedance is purely real. At higher frequencies the reactance is dominated by the inductor (it is positive) while at lower frequencies it is dominated by the capacitor (it is negative).

The transfer function, or voltage gain, of the RLC circuit alone is given by

$$G_V^{\text{RLC}}(\omega) = \left|\frac{V_{\text{out}}(\omega)}{V_{\text{in}}}\right| \tag{3.1.4}$$

$$= |i\omega C Z(\omega)|^{-1} \tag{3.1.5}$$

$$= \left|1 - \left(\frac{\omega}{\omega_0}\right)^2 + \frac{i}{Q}\frac{\omega}{\omega_0}\right|^{-1} . \tag{3.1.6}$$

This function is completely determined by the reduced frequency ω/ω_0 and the quality factor Q. The transfer function is equal to 1 at $\omega = 0$ (i.e. in DC) and tends to zero as $\omega \to \infty$. For convenience, $G_V^{\text{RLC}}(\omega)$ is plotted as a function of various values of Q in Fig. 3.1.

Since the transfer function has a second order polynomial denominator, it has two complex poles located at

$$\omega_{a,b} = \pm\omega_0\sqrt{1 - \frac{1}{4Q^2}} + i\frac{\omega_0}{2Q} . \tag{3.1.7}$$

If $Q \leq \frac{1}{2}$ the poles are both purely imaginary and the oscillator is said to be *over-damped* (or just *critically damped* if the equality holds). Under these conditions the resonator does not oscillate. When over or critically damped, indeed, the resonator's dissipations consume all the energy in less than one cycle. From now on, it is assumed that $Q > \frac{1}{2}$ (under-damped case). It is also curious to note that, when $Q > 1/2$, $|\omega_{a,b}(Q)| = |\omega_0|$. This means that sweeping Q in the range $[1/2, \infty]$, the root locus of the
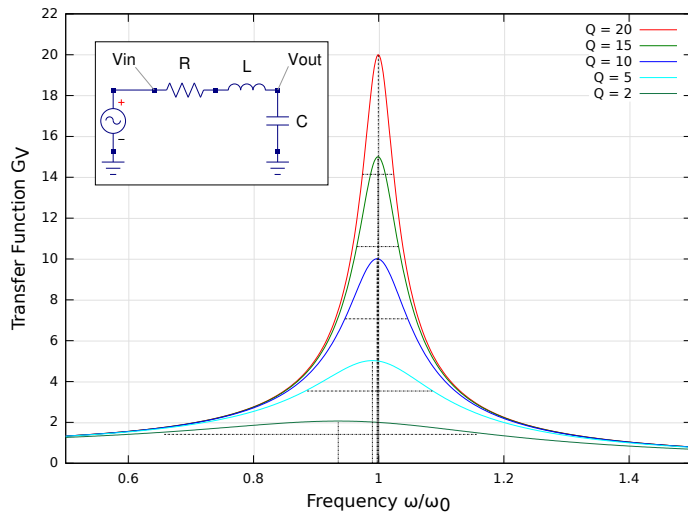
Figure 3.1: Transfer function of the RLC resonator (circuit shown in the inset) as a function of frequency and Q. For high Q the peak frequency tends to ω_0 and the bandwidth is ω_0/Q.
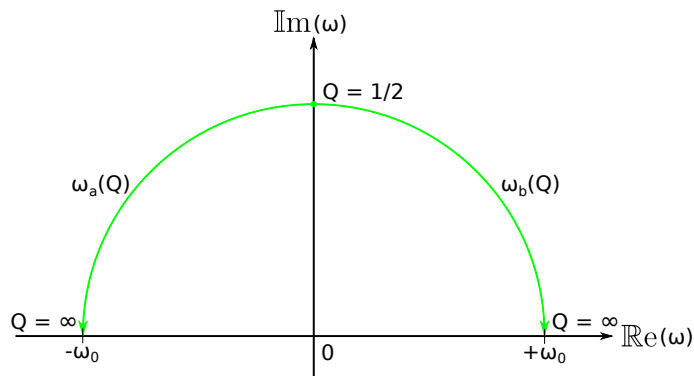

Figure 3.2: The root locus of the transfer function's poles, as a function of the parameter Q. In the limit of big Q, $\omega_{a,b} \rightarrow \pm\omega_0$. Since the frequency of the RLC circuit can only be purely real and positive, the projection of ω_b determines the *natural frequency* of the circuit. This frequency tends to ω_0 as $Q \rightarrow \infty$.

poles draws a semicircle around the origin in the positive imaginary part of the complex plane (Fig. 3.2). The poles get closer to the real axis when Q increases.

The maximum of the transfer function Eq. 3.1.6 does not occur at the resonant frequency, but rather at the slightly lower so-called *peak frequency*. This is given by

$$\omega_{\mathrm{p}} = \omega_0 \sqrt{1 - \frac{1}{2Q^2}} \ . \tag{3.1.8}$$

The reason why the peak frequency is lower than the resonant frequency can be understood by thinking of the mechanical analogue of the forced swing. Driving the swing, the oscillation amplitude is bigger than in the free case. If a damping force (the viscosity of air for the swing) is acting, then the oscillation period is longer and dependent on the amplitude.

The voltage gain exactly on resonance is

$$G_V^{\mathrm{RLC}}(\omega_0) = \frac{1}{\omega_0 C R} = \frac{\omega_0 L}{R} = Q \tag{3.1.9}$$

but it is maximum at the peak frequency

$$G_V^{\mathrm{RLC}}(\omega_{\mathrm{p}}) = \frac{Q}{\sqrt{1 - \frac{1}{4Q^2}}} \ . \tag{3.1.10}$$

However, the factor $\sqrt{1 - \frac{1}{4Q^2}}$ leads to corrections of less than 1% when Q is bigger than 4, and less than 0.1% when Q is bigger than 12. For this reason, even with modest Q, it is reasonable to approximate ω_0 as the peak frequency and Q as the maximum gain. It can be shown that, with high Q, the -3dB-voltage-bandwidth is given by

$$\Delta\omega_V = \frac{\omega_0}{Q} \ . \tag{3.1.11}$$

All these results are summarized in the plot Fig. 3.1. In this section the resonator's relevant parameters have been calculated and the underlying physics explained in the ideal case where a matching network is not present. On resonance, however, the impedance of the RLC circuit - which is given only by R (Eq. 3.1.3) - is often smaller than the source impedance. For this reason a matching network is necessary, and in the next section this is reintroduced and the calculations are corrected.

3.1.3. Matched resonator

As discussed in Sec. 2.4, different kinds of matching can be used. For simplicity - because of the ideal broad bandwidth it has - only the transformer will be considered here. Other kinds of matching circuits give the same results as the transformer, provided that the bandwidth of the matching is bigger than the bandwidth of the resonator itself (i.e. k is almost frequency-independent for frequencies close to ω_0).

The transformation ratio (Eq. 2.4.4) used to match the circuit on resonance is given by

$$k^2 = \frac{|Z(\omega_0)|}{|Z_s|} = \frac{R}{Z_s} \ . \tag{3.1.12}$$

With this transformation, which is frequency-independent for an ideal transformer[1], the "matched" impedance of the amplifier becomes

$$Z^{\mathrm{M}}(\omega) = \frac{Z(\omega)}{k^2} = Z_s \left[1 + iQ \left(\frac{\omega}{\omega_0} - \frac{\omega_0}{\omega} \right) \right] \ . \tag{3.1.13}$$

The adjective "matched" is properly said only on resonance, where $Z^{\mathrm{M}}(\omega_0) = Z_s$. For different frequencies this relation is not true, thus the voltage applied to the "matched" resonator by the source is frequency-dependent. If V_s is the voltage generated inside the voltage source (in the source's Thevenin equivalent), on resonance the voltage applied to the amplifier is $V_s/2$. At much lower or higher frequencies, where the resonator is completely unmatched ($Z^{\mathrm{M}}(\omega) \gg Z_s$), the voltage applied is V_s.

With reference to Fig. 3.3, it is convenient to write the voltage gain as

$$G_V^{\mathrm{M}}(\omega) = \left| \frac{2V_{\mathrm{out}}(\omega)}{V_s} \right| \tag{3.1.14}$$

and not as

$$G_V^{\mathrm{M}}(\omega) = \left| \frac{V_{\mathrm{out}}(\omega)}{V_{\mathrm{in}}(\omega)} \right| \tag{3.1.15}$$

because V_s is frequency independent. In this way $G_V^{\mathrm{M}}(\omega)$ has the same shape as $V_{\mathrm{out}}(\omega)$, as seen on the oscilloscope. Moreover, Eq. 3.1.14 is the equation used in any network analyzer when measuring the linear gain from the scattering parameter S_{21}. Provided that

$$V_{\mathrm{in}}(\omega) = V_s \frac{Z^{\mathrm{M}}(\omega)}{Z^{\mathrm{M}}(\omega) + Z_s} \tag{3.1.16}$$

---

[1] In an ideal transformer, the voltage transformation depends only on the ratio of the windings in the two coils. In a real transformer this is not true because the magnetic flux transfer is frequency-dependent.
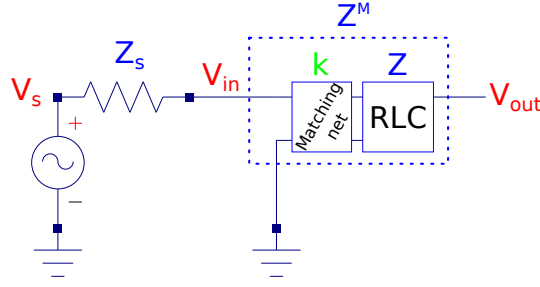
Figure 3.3: Complete circuit scheme of the matched voltage amplifier. Since Z^{M} is frequency-dependent, so is V_{in}.

and that

$$V_{\mathrm{out}}(\omega) = \frac{kV_{\mathrm{in}}(\omega)}{i\omega C Z^{\mathrm{M}}(\omega)k^2} \tag{3.1.17}$$

after some algebra it is easy to find

$$G_V^{\mathrm{M}}(\omega) = \frac{kQ}{\frac{\omega}{\omega_0}\left|1 + \frac{iQ}{2}\left(\frac{\omega}{\omega_0} - \frac{\omega_0}{\omega}\right)\right|} . \tag{3.1.18}$$

The maximum gain appears at the same resonance frequency (in the high-Q approximation), and it is now given by

$$G_V^{\mathrm{M}}(\omega_0) = kQ = \frac{\omega_0 L}{\sqrt{Z_{\mathrm{s}}R}} . \tag{3.1.19}$$

When the resonator is matched, the voltage gain is thus different from the unmatched case. It is reduced by a factor k, and so it is not possible to calculate it knowing only the quality factor: one must either additionally know R, C or L, or $G_V^{\mathrm{M}}(\omega_0)$ must be measured experimentally. Conversely, it is possible to calculate Q directly from the bandwidth of the transfer function, even in the matched case. In a similar way to the unmatched case, it is possible to show that the $-3\mathrm{dB}$-voltage-bandwidth is given by

$$\Delta\omega_V = \frac{2\omega_0}{Q} . \tag{3.1.20}$$

The matching network has the side-effect of increasing the bandwidth by a factor 2.

3.1.4. Measuring the quality factor

The quality factor Q is an important parameter to characterize a resonator (see Sec. 3.1.1). To offer maximum flexibility under various experimental constraints, it can be useful to have a variety of methods to measure it, possibly with different instruments. Such a variety of methods is indeed possible. Thinking of the matched resonator as a circuit with one input port and one output port, it is possible to measure Q from either port, independently. Below two methods are summarized for convenience:

1. At the output port, sweeping the input frequency and monitoring the output with an oscilloscope, it is possible to plot the voltage gain as a function of frequency. A network analyzer can be used as well, provided that it can measure the S_{21} parameter - i.e. the linear gain. Measuring the bandwidth of the resonance, where $G_V^{\mathrm{M}}(\omega) = G_V^{\mathrm{M}}(\omega_0)/\sqrt{2}$, with the use of Eq. 3.1.20 one can calculate Q as

$$Q = 2\frac{\omega_0}{\Delta\omega_V} \ . \tag{3.1.21}$$

   This first method is particularly convenient, since it allows the measurement of Q and G_V with the same instrument.

2. At the input port, with the use of a network analyzer, it is easy to measure the scattering parameter as a function of frequency. From Eqs. 3.1.13 and 2.4.9, it is possible to find the scattering parameter S

$$S(\omega) = \frac{iQ\left(\frac{\omega}{\omega_0} - \frac{\omega_0}{\omega}\right)}{2 + iQ\left(\frac{\omega}{\omega_0} - \frac{\omega_0}{\omega}\ .\right)} \tag{3.1.22}$$

   Its magnitude is equal to 1 for $\omega = 0$ and $\omega = \infty$, and it is equal to 0 on resonance (evidence for perfect matching). The bandwidth of the notch can be found equating $|S|^2$ to $1/2$. Solving the equation, the difference between the two positive solutions is

$$\Delta\omega_S = \frac{2\omega_0}{Q} \ . \tag{3.1.23}$$

   Thus, measuring the bandwidth where $|S| = 1/\sqrt{2}$, one can calculate Q as

$$Q = 2\frac{\omega_0}{\Delta\omega_S} \ . \tag{3.1.24}$$

   The convenience of this method is that it requires only one port for the measurement, as opposite to the first measurement where both ports must be connected to the instrumentation.

For both methods the relevant bandwidth is thus the one where the maximum value of S or G_V^{M} drops down by a factor $\sqrt{2}$ from the maximum, and in both cases Q is twice the ratio of the resonance frequency over the bandwidth.

3.2. Components selection

In order to judge whether the requirements given in Sec. 2.2 can be satisfied or not, it is still necessary to find the right components to build a working resonator. This section describes the component's limiting factors, from the underlying physics to how these can be practically taken into account. The operation principles of an RLC amplifier described in the previous section (Sec. 3.1) can be used to optimize the choice.

3.2.1. Limiting physics

From the definition of quality factor Eq. 3.1.1, it is evident that to improve Q one has to reduce dissipations. For an inductor, dissipations come mainly from the resistance of the coil and the hysteresis losses in the core, while for a capacitor they come mainly from leakage currents in the dielectric. In addition, there are three other significant effects that increase these resistances: self-resonance, skin effect and proximity effect [39].

The *self-resonance frequency* (SRF) is the frequency at which the component will start to resonate by itself as a parallel or series RLC resonator, yielding to very high impedances and dissipation. The self-resonance come from the presence of both a capacitive and an inductive part in every real component. In an inductor, for example, the capacitance comes from the coupling between the windings, and can be diminished by increasing the pitch between windings. For frequencies higher than the SRF, the component stops working as it should and it becomes the opposite kind of reactance (inductors become capacitors and vice-versa). The SRF will vary from component to component, depending on the construction details (shape and dimensions). Every component must be chosen so that the SRF is much greater than the operating frequency ω_0.

The second important effect, especially for radio-frequency components, is the *skin effect*. This effect limits the current in the center of a conductor, and it is due to the electromotive force induced by the alternating magnetic field, which is generated by the current itself. The overall effect is that the current density distributes near the surface (the "skin") of the conductor reducing the conductive area and, thus, increasing the resistance. The skin depth is the averaged depth from the surface at which the current flows, and it is described by

$$\delta(\omega) = \sqrt{\frac{2\rho}{\omega\mu}} \tag{3.2.1}$$

where ρ is the material's electrical resistivity and μ the relative permeability. For copper at room temperature the skin depth is equal to

$$\delta(\nu = \omega/2\pi) = \frac{6.6 \cdot 10^{-2}}{\sqrt{\nu}} \, \mathrm{m}\sqrt{\mathrm{Hz}} \qquad (3.2.2)$$

which is just $21 \, \mu\mathrm{m}$ at $10 \, \mathrm{MHz}$. At high frequencies, the increase in resistance is thus proportional to the square root of the frequency. With a wire diameter of $0.5 \, \mathrm{mm}$ and a frequency of $10 \, \mathrm{MHz}$, the resistance is increased by a factor of 6 just because of this effect.

The last degrading effect is called the *proximity effect*. It is similar to the skin effect, as it describes the eddy currents induced by an alternating current into nearby conductors. Since all these induced currents will dissipate energy, the overall effect for the original current is an increased net resistance. As for the skin effect, the increase in resistance is proportional to the square root of the frequency.

3.2.2. Reactive component's quality factor

In every non-ideal component some effective resistance is always present and it always dissipates some power. In order to choose the proper components for the resonator, it is important to have a useful way to handle these dissipations. This can be done by means of another quality factor Q_x for every reactive component X. For a complex impedance $Z = R + iX$ (a reactance with an equivalent resistance in series), this parameter is defined as

$$Q_\mathrm{x} = \frac{X}{R} \, . \qquad (3.2.3)$$

The definition comes from Eq. 3.1.1, and it is very useful in the case of a resonator because, on resonance, the reactances of the capacitor and the inductor are equal. Since the total R of the resonator is given by the sum of the two effective resistances of the capacitor and the inductor, it is possible to write

$$\frac{1}{Q} = \frac{1}{Q_\mathrm{C}} + \frac{1}{Q_\mathrm{L}} \, . \qquad (3.2.4)$$

The component with the lowest Q_x will contribute the most to the total R of the resonator. If the Q_x factor of one component is much less than that of the other components, than the quality factor of the resonator Q is dominated by this lowest Q_x.
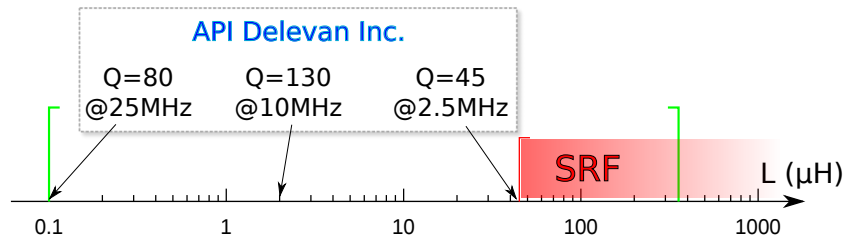
Figure 3.4: Scheme of the suitable, available inductors. Inductors with inductance bigger than $33\,\mu$H have an SRF lower than 30 MHz, which is too close to the desired operating frequency. In all the range, the highest Q_L are obtained by *API Delevan*.

3.2.3. Choice(es)

Using the component's quality factor and the equations in Sec. 3.1, R, L and C have to be determined for the specific application of the resonant voltage amplifier. Both the Q_x and the SRF change from component to component so that they have to be specified on datasheets.

It is convenient to look for the right components starting from the capacitor. In an RLC circuit like Fig. 2.9, the capacitance C is given by the capacitance of the trap ($\sim 1\,$pF) and that of any other capacitors added. In order to measure the voltage at the output port of the resonator without affecting (loading) the circuit itself with the instrumentation, it is necessary to use a voltage divider, more precisely a capacitive divider (Sec. 4.2). For this reason, at least one extra capacitance will be added to the resonator. Provided that the capacitor has to be RF compatible, high voltage ($\sim 100\,$V) compatible and as stable as possible with the expected temperature changes ($4-300\,$K), the only choice is to use a capacitor with mica or ceramic dielectric. Standard components of this kind have capacitances ranging between $1\,$pF and $1\,$nF. The mica capacitors that were chosen (because of immediate availability) are produced by *Cornell Dubilier Electronics*. These components are small SMD devices, and the datasheet states that the quality factor is > 1000 at $10\,$MHz. The SRF is $> 100\,$MHz for the $1\,$nF capacitor and $> 1\,$GHz for capacitors smaller than $10\,$pF. In addition, the maximum allowed voltage is $500\,$V and the temperature coefficient is less than $100\,$ppm/℃ (to be tested at low temperature). These capacitors are therefore suitable for the amplifier's requirements stated in Sec. 2.2.

Once a range for C is found, the value for the inductance is constrained by the resonant

frequency. As said in 2.2, the resonance frequency must be chosen between 7 and 16 MHz. At lower frequencies the well depth will not be deep enough to trap and at higher frequencies breakdown (due to the high requested voltages) will likely happen. With these ranges of C and ω_0, the inductance is constrained to the range between 100 nH and 260 μH. Inductors which are available on the market (*Farnell, DigiKey, Mouser and RS-Components*) as standard components have, in the prescribed range, self-resonance frequencies very close to, or even lower than, the operating frequency. The SRF is roughly inversely proportional to the inductance. Requiring a SRF of at least 30 MHz - which is reasonable since it is twice the maximum frequency at which the resonator will be operated - the biggest available inductance is of only 33 μH. In this range, the company which sells inductors with the highest quality factors is *API Delevan Inc.* In Fig. 3.4 a scheme of the available inductors is presented. The materials used for the inductors' cores are usually iron, ferrite or phenol, though the latter has a much lower Q_L. The testing frequency, which is roughly the intended operating frequency, is decreasing with increasing inductance. For frequencies near 10 MHz the best inductances are of order 1 μH and can have quality factors Q_L around 100. In any case, the inductor's quality factor is much less than the capacitor's quality factor, which means that the total Q of the resonator will be completely determined by the inductor.

Looking at Fig. 3.4, one could think that the best choice is the 2.2 μH inductor, because of its high quality factor $Q_L = 130$. However, when putting the numbers in Eq. 3.1.19, the result is only $G_V^M = 19.0$ at $\omega_0 = 2\pi \cdot 10$ MHz. This gain is less then the lower limit - $G_V > 20$ - imposed in Sec. 2.2. The problem, here, is that the equivalent resistance is too low, only 1.1 Ω, and that the matching network has to lower the voltage by a factor $\sqrt{R/Z_s} = 0.15$. To choose more carefully the proper inductor, it is better to rewrite the voltage gain in Eq. 3.1.19 as

$$G_V^M(\omega_0) = \sqrt{\frac{\omega_0 L Q_L}{Z_s}} \ . \tag{3.2.5}$$

Written in this way it is obvious that, to achieve a high voltage gain, it is not sufficient to choose the highest Q_L but it is also very important to choose high inductances. By contrast, the frequency has still to be small ($\sim$ 10 MHz), as the required voltage in Eq. 2.1.11 is quadratic in the frequency (see Fig. 2.5). As a comparison, the voltage gain of the three inductor shown in Fig. 3.4, is summarized in Tab. 2. Here two possible assumptions are made: for G_V^M I the quality factor is thought to be the same at the testing frequency (stated in the datasheet) and at 10 MHz. For G_V^M II the quality factor is assumed to be linear in the frequency, as prescribed by Eq. 2.3.7 when R is constant. As can be seen, in both the approximations the only inductor which satisfies the requirement of the minimum voltage gain is the one with the highest inductance.

Inductor	Q_{L}	G_V^{M} I	G_V^{M} II
100 nH	80@25 MHz	3.17	2.01
2.2 μH	130@10 MHz	19.0	19.0
33 μH	45@2.5 MHz	43.2	86.4

Table 2: A comparison of the voltage gain achievable with three real inductors at 10 MHz. In the third column the quality factor is assumed to be the same at the operating frequency and at the testing frequency. In the last column the quality factor is assumed to be linear with the frequency.

3.3. Optimization and cures

In the theory developed so far, some implicit assumptions were made: firstly, that the optimal frequency at which the circuit is matched is the peak frequency. Secondly, that no further constraint limits the choice in the matching circuit. These assumptions are in contrast with another important factor to take in consideration in the case of an ion-trap. In order to remove any DC bias voltage and reduce the low-frequency noise on the RF electrodes, which could perturb the ions, a DC path to ground for the trap should be provided. With this new feature in mind, the previous assumptions must be revised. In particular, it must be noted that on resonance the impedance is purely real and generally smaller than $Z_{\mathrm{s}} = 50\,\Omega$. This, in turn, means that the impedance of the resonator lies, on resonance, in the third region of the Smith chart (Fig. 2.12). In this region, if the simple "L-section" (Fig. 2.13) is used to match, the first impedance must be put in series with the circuit and the second impedance, which has to be the opposite type of reactance with respect to the first, in parallel. An example of this matching can be seen in Fig. 3.5. In this picture, the green line represents the scattering parameter S, and the black dot represent the resonance frequency. Because of the capacitor, the two matching circuits do not provide a DC path to ground other than through the voltage supply. Some, but not all, voltage supplies provide a DC path to ground. For robust and general operation, it would be good to not have to rely on this, but rather include a DC path to ground in the matching circuit. A different kind of matching, like the use of a transformer, can avoid this, but with the addition of significant difficulties in the design (because it is not easy to tune the voltage transformation of a transformer).

An interesting observation comes to help at this point. The path followed by $S(\omega_0)$ on the Smith chart when the first impedance is added, follows exactly the plot of $S(\omega)$. This means that the role of the first impedance is nothing more than shifting all the frequencies upwards (inductor) or downwards (capacitor). Doing so, the old resonance
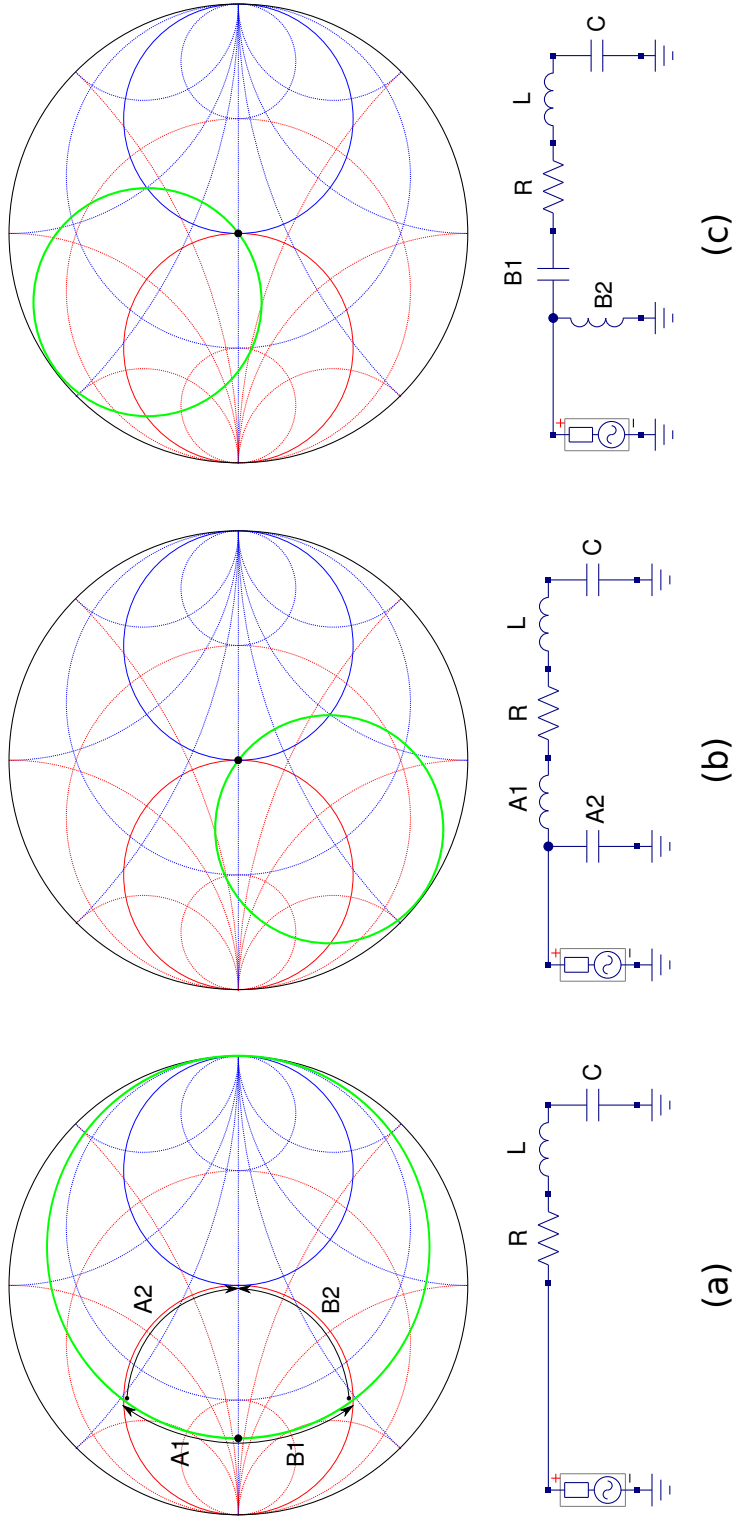
Figure 3.5: The green line represents the scattering parameter S as function of frequency (clockwise rotation with increasing frequencies). A resonator with $R < Z_s$ is always in the third zone of the Smith chart on resonance (the black dot mark the resonance frequency). To match the circuit (a), two opposite reactances must be used, as shown in (b) or (c). The first one is always in series. The path followed by the resonance during the match is depicted with the arrows in (a).
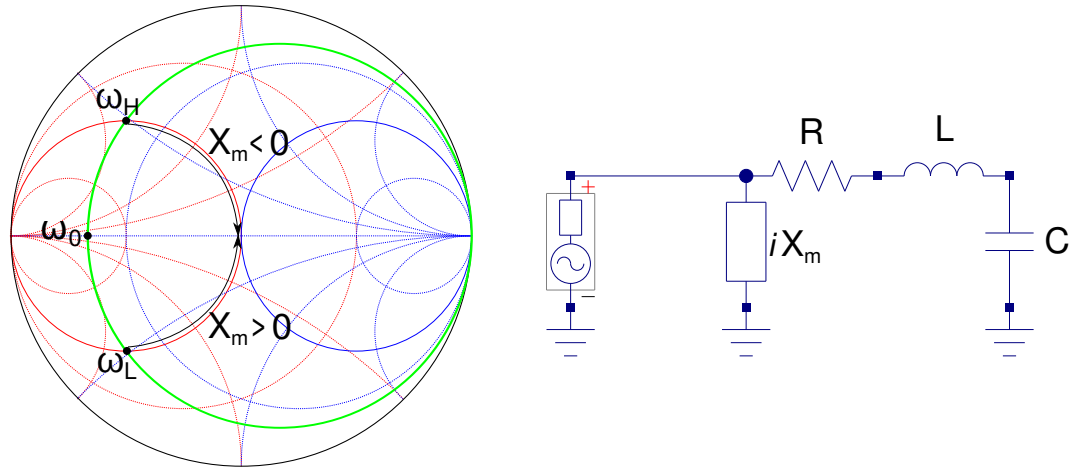
Figure 3.6: A series resonator can be matched with the use of only one reactance if matched out of resonance. When matched at ω_H a capacitor should be used. When matched at ω_L, an inductor should be used.

frequency is not on resonance anymore ($S(\omega_0) \notin \mathbb{R}$), but lies at the crossing point with the unitary circle connected to the center of the Smith chart (the perfect matching). From there, and adding the proper parallel reactance, the matching can be achieved. Exploiting this observation it is possible to find an alternative to the "L-matching". The idea is to remove the first reactance, and match at an higher (ω_H) or lower (ω_L) frequency instead that at resonance (Fig. 3.6). These two frequencies are found at the crossing point between $S(\omega)$ and the unitary circle in the admittance Smith chart, where the following relation holds

$$\frac{1}{Z_s} = \frac{1}{Z(\omega_{H,L})} + \frac{1}{iX_m(\omega_{H,L})} \tag{3.3.1}$$

where $X_m(\omega_{H,L}) \in \mathbb{R}$ is the parallel matching reactance. In Appendix A the calculation for solving the above relation are given, and the important results are reported here in Tab. 3. The most important result is the voltage gain: even if the matching was done at a non-optimal frequency - i.e. not on resonance - the maximum gain is not significantly affected by this choice. In conclusion, a much easier matching can be achieved if a frequency different from the resonance is chosen. This match does not change the gain and if done at ω_L it also provides a DC path to ground for the trap through the matching inductor.

	$\alpha :=$	$\frac{Z_{\mathrm{s}}}{R} - 1$

Inductor		
	$\omega_{\mathrm{L}} =$	$\omega_0 \sqrt{1 - \frac{-\alpha}{4Q^2}} - \frac{\omega_0}{2Q}\sqrt{\alpha}$
$X_{\mathrm{m}}(\omega_{\mathrm{L}}) =$	$\frac{Z_{\mathrm{s}}}{\sqrt{\alpha}}$
$G_V(\omega_{\mathrm{L}}) =$	$\frac{\omega_0}{\omega_{\mathrm{L}}}G_V(\omega_0)$

Capacitor		
	$\omega_{\mathrm{H}} =$	$\omega_0 \sqrt{1 - \frac{-\alpha}{4Q^2}} + \frac{\omega_0}{2Q}\sqrt{\alpha}$
$X_{\mathrm{m}}(\omega_{\mathrm{H}}) =$	$-\frac{Z_{\mathrm{s}}}{\sqrt{\alpha}}$
$G_V(\omega_{\mathrm{H}}) =$	$\frac{\omega_0}{\omega_{\mathrm{H}}}G_V(\omega_0)$

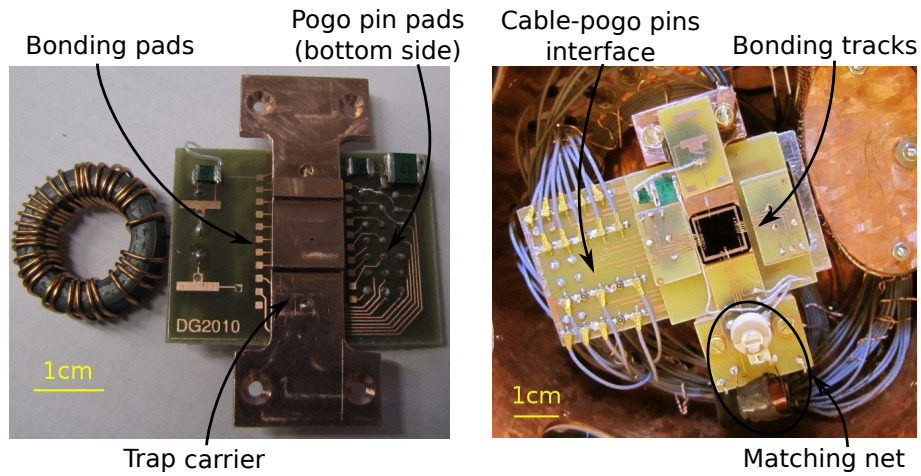Table 3: Relevant equations for the matching with only one parallel reactance.

Figure 3.7: The first and the last PCB, codename "Shy" and "SCairy". During the development, more layers were added and different bugs were ruled out. In the last design the resonator's PCB is only three centimeter wide. In this way it fits also in the liquid helium dewar for a quick and low-temperature test.

3.4. PCB development

The last step in the design of the trap-drive resonator, is the development of a printed circuit board (PCB) which can easily interface with the trap. This PCB should be small enough to fit into the cryostat, but at the same time it should be big enough to provide not only the RF signal but also 16 DC signals for the segmented electrodes. Like everything else, it should be ultra high vacuum and cryogenic compatible. The common choice is thus the use of *Rogers* RO3003 [35] as the PCB insulation material, but for the earlier stage of development, the usual *NEMA*[2] FR-4 was used to produce "home-made" PCBs. In addition, any electrical contact should be made with solder, bonding wires or with pogo pins [40]. Other kind of contacts or connectors should be avoided (or at least carefully tested): if the thermal contraction of the female receptacle is lower than the thermal contraction of the male conductor, electrical contact can be lost during the cooling cycle. During this thesis project, four different PCB designs were made, starting from a simple, double-layer PCB, ending with a more complicated stack of four PCBs one on top of the other (Fig. 3.7). The problems that were encountered at various stages, and that were fixed in subsequent versions, are:

---

[2]National Electrical Manufacturers Association

- the unshielded RF track, running from the end of the coaxial cable to the trap electrodes, has to be as short as possible. This limits RF pickups by the DC cables;

- the pads for the gold-wire bonding (the thin wires which connect the PCB and the trap) have to be slightly below the trap surface and half a centimeter away from the side of the trap carrier. If this condition is not satisfied, it is not geometrically possible to bond the wires with our bonding machine;

- the copper tracks have to be quite symmetric. This means that the top and bottom layers have to show more or less the same amount of copper, distributed roughly homogeneously. If not, since the thermal expansion of copper and of FR-4 are not the same, the PCB will bend, eventually breaking or interrupting some connections;

- the pogo pins are more stable when placed directly below the trap carrier. In this way their force will be absorbed by the bulky copper mount and will not stress/bend the PCB;

- two cables should be used for each electrode, when possible. In this way it is possible to do some continuity measurement and search for broken connections, no matter if in air or in vacuum.

Especially in the latest version, the dimensions of the resonator's PCB where kept very small. This was done in order to have a separate PCB which could be put in a liquid helium bath for a rapid low-temperature test. During this procedure, fine tuning of the matching circuit can be achieved.

3.5. Summary

Topic of this chapter was the design of the RF amplifier. It covered all the different aspects, from the general theory - used as a guide to an optimized components selection - to some attentions for a robust trap drive, finishing with some tips to bear in mind when drawing the PCB. The step from theory to practice will be covered in the next chapter, where the experimental realization and testing of several resonators is reported. The final resonator satisfied all the requirements given in Sec. 2.2 and it was used, successfully, to trap ions.

4. Experimental testing

A total of six different resonators were built and tested, at room and cryogenic temperatures. This fourth chapter describes the experimental results obtained in the laboratory. In Sec. 4.1 a short explanation of the cryostat - which type, its features and why it is necessary for this experiment - is reported. In the following Sec. 4.2 the probe for the resonator - a capacitive divider - is introduced and the calibration curves given. From Sec. 4.3 to Sec. 4.7 the circuits are presented with their design features, and the room temperature and cryogenic temperature results are shown. These results are also summarized in a table at the end of this chapter.

4.1. The cryostat

A long-term goal of this experiment is the measurement of the anomalous heating rate [41, 42, 43] for various planar surface ion-traps. This electric-field noise (S_E) source is the main concern when scaling traps to smaller dimensions, as its spectral density quickly increases with decreasing ion-electrode distance d

$$S_\mathrm{E}(\omega_0) \propto d^{-4} \ . \tag{4.1.1}$$

It has been shown that this effect is thermally activated [24, 44], and that cooling the trap electrodes to cryogenic temperatures could reduce the noise by seven orders of magnitude (with respect to the same trap at room temperature). For this experiment a closed-cycle cryostat was used and, as explained in Sec. 2.2, the final resonator should be both vacuum and cryogenic compatible. The heart of the cryostat is a two stage Gifford-MacMahon cryo-cooler, manufactured by *ARS - Advanced Research Systems, Inc.* (model DE-210SF). As shown in the schematic, Fig. 4.1, the trap and the resonator are mounted inside two radiant heat shields, the first connected to the first cooling stage (at $\sim 60\,\mathrm{K}$), and the second connected to the last cooling stage (at $4\,\mathrm{K}$). The windows mounted on the shields are IR-reflecting coated. They provide the necessary optical access to the trap, thus limiting the radiant heat load (compared to a simple hole without windows). In the direction of the Ca source, where windows are not suitable, the radiant heating can be kept low by reducing the size of the orifice for the atomic beam (diameter $3\,\mathrm{mm}$). The cryocooler's specifications state that the minimum temperature achievable is $< 4\,\mathrm{K}$ and that the cooling power at this temperature is $500\,\mathrm{mW}$. With this setup, the minimum temperature achieved was $4.9\,\mathrm{K}$ (measured at the trap carrier with a Si diode), obtained during the testing of the last PCB, SCairy. Another important consideration for reliable quantum coherent operations is the trap vibrations. These vibrations were measured during a preliminary test to be $100\,\mathrm{nm}$ in amplitude. The
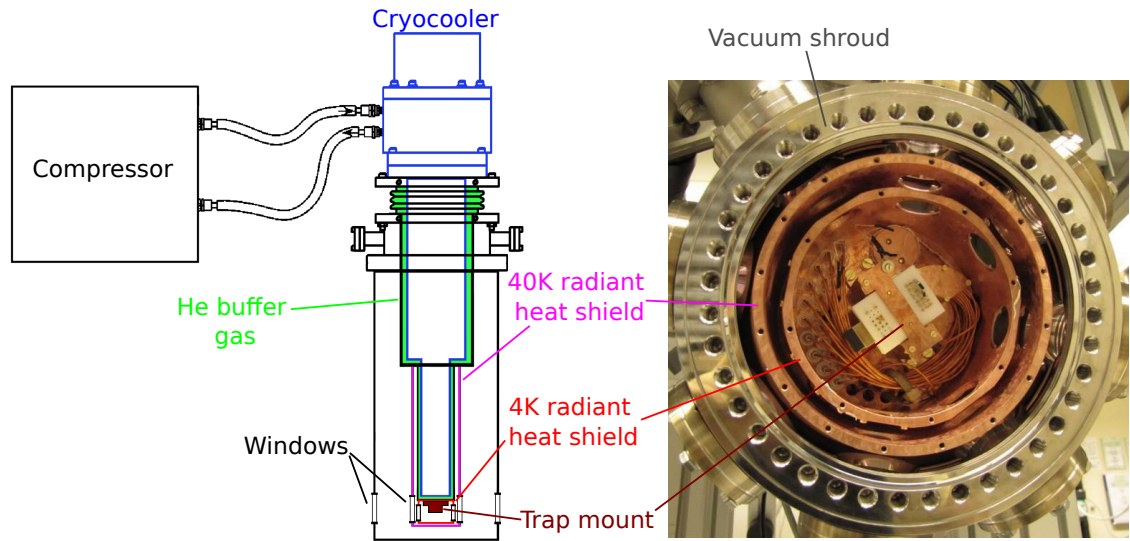
Figure 4.1: Cryostat schematic. The trap and the resonator are mounted on the trap mount, inside the 4 K radiant heat shielding.

buffer gas (helium) separating the cryocooler from the vacuum chamber is necessary to provide heat transport while mechanically decoupling the two parts.

For every resonator, the testing procedure consisted in:

- mounting the circuit in the cryostat (and eventually tuning the matching network);

- closing the vacuum chamber;

- pumping out the chamber with a rotary pump and a turbomolecular pump (manifactured by *Pfeiffer Vacuum GmbH*), to a pressure of about 10^{-6} mbar;

- cooling down the cryostat to the minimum temperature.

4.2. Capacitive divider

If the voltage output of the resonator on the trap electrodes needs to be measured, it is necessary to use an instrument which will not influence the circuit itself. The requirement for this is that the input impedance of the instrumentation has to be much larger than the output impedance of the resonator itself. The use of an oscilloscope-probe usually removes this problem, but for this sensitive application the parasitic capacitance of the
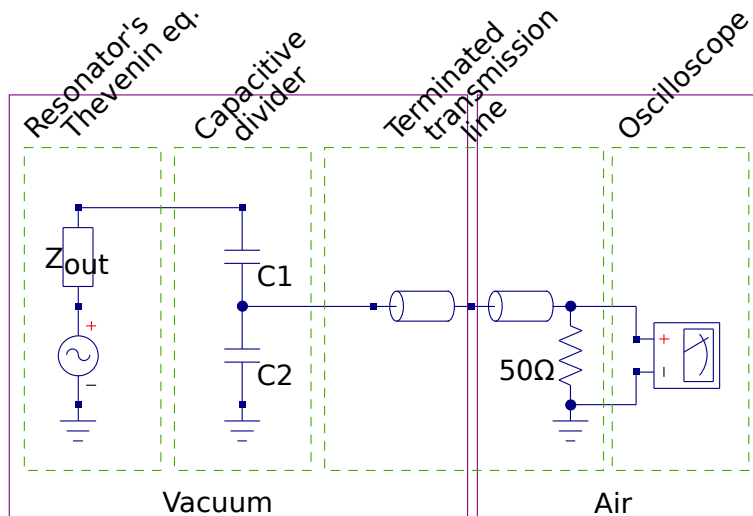
Figure 4.2: Because of the high output impedance of the resonator (it is the same as the input impedance of a parallel RLC resonator) particular attention should be paid to the measuring set up. Using a voltage divider, such as a capacitive divider, it is possible to increase the input impedance of the measuring apparatus. The drawback is a reduced voltage amplitude measured at the oscilloscope, which has to be corrected for the data-analysis. The values used for the two capacitors are $C1 = 5\,\mathrm{pF}$ and $C2 = 1\,\mathrm{nF}$, thus providing a transformation ratio of ~ 200.

probe was still too big compared to the capacitance of the resonator. A capacitive divider (Fig. 4.2) was thus adopted to provide a $\sim 200\times$ impedance magnification and reduce the unwanted loading. Since the measured voltage is reduced by the same amount, every measurement must be corrected accordingly.

The mica capacitors used for this application are manufactured by *Dubilier Electronic* (Sec. 3.2.3). The smaller capacitance was chosen to be $C1 = 5\,\mathrm{pF}$. This value is small enough not to overload the circuit[3] and at the same time is not so small as to be affected by the capacitance of the PCB tracks. The bigger capacitance was then chosen to be $C2 = 1\,\mathrm{nF}$, i.e. 200 times bigger. Ideally, the transformation ratio between the input voltage and the output voltage of the divider should be constant with the frequency.

---

[3]Here "overload" means critically compromising the resonator's characteristics, such as quality factor or voltage gain. Nevertheless it is obvious that when calculating the total capacitance of the resonator, the capacitance of the divider is not negligible.
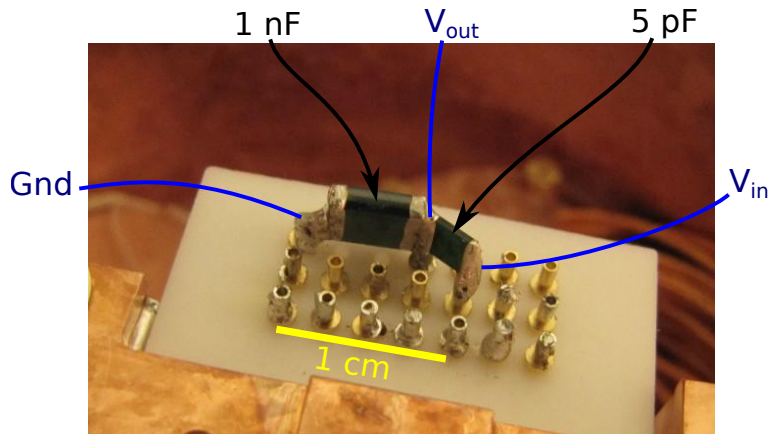
Figure 4.3: The capacitive divider built directly on the pogo pin counter-contacts, ready to be cooled. The unshielded leads include the contacts, the pogo pins (not visible) and the unshielded part of the coaxial cable (not visible). The total leads length is about 5 cm.

However, since the voltage measurement is done outside the cryostat through a long coaxial cable, it is necessary to terminate the cable with a $50\,\Omega$ terminator. If the cable is not terminated, its capacitance - and thus the ratio of the divider - will depend on the cable length. When terminated this dependence is eliminated, but at the same time the divider's ratio becomes frequency-dependent. It is thus important to measure this ratio as function of the frequency, for both high and low temperatures.

For the test inside the cryostat, the small circuit was built soldering the capacitors directly across the connectors which were going to be placed in contact with the pogo pins (see Fig. 4.3). In this way the unshielded wires connecting the capacitors to the coaxial cable were as short as possible. Despite this precaution, the leads were not shorter than 5 cm. A similar measurement was performed with a much shorter length of the leads (about 1 cm), both outside the cryostat and in a bath of liquid helium (4.2 K).

In Fig. 4.4 the calibration curves are reported. The measurement agrees with the predicted behavior for frequencies lower than $\sim 11\,\mathrm{MHz}$, then it starts to increase whereas theoretically it should keep going down. A $\pm 10\%$ systematic error arises in different dividers from the uncertainty on the capacitors' values, while another systematic error of -9% shifts the calibration curves (below $11\,\mathrm{MHz}$) from the theoretical line. At the highest frequencies, a non-ideal behavior is evident. This effect is probably due to some parasitic reactance given by the components' leads, since it is less pronounced in the
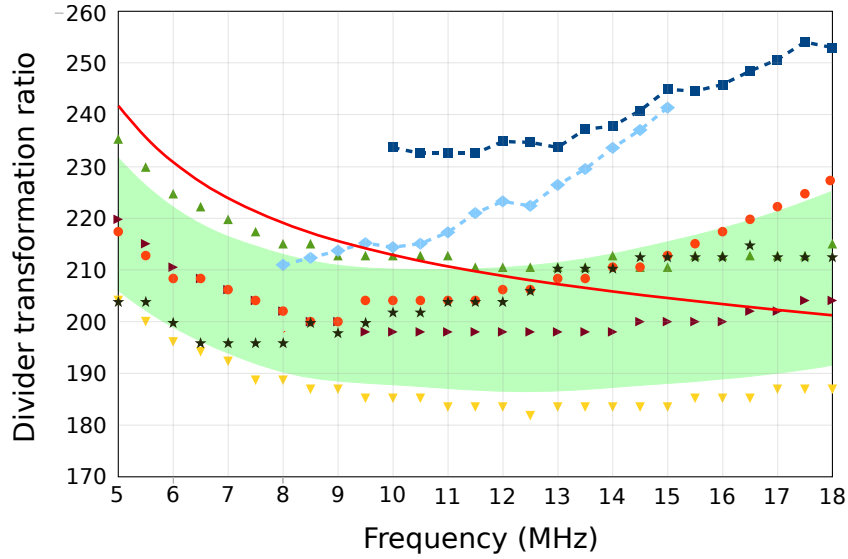
Figure 4.4: Experimental calibration of the capacitive divider. The instrumental uncertainty affecting the transformation ratio is given by the symbol dimension. The uncertainty in the frequency measurement is negligible. The triangle-shaped data-points were taken with different capacitors, soldered as close as possible to the end of the BNC cable (test done outside the cryostat). The star-shaped data-points were taken in the same manner, but in a bath of liquid helium, at 4.2 K. The circle-shaped data-points were taken with the same setup but with 5 cm long leads for both capacitors. The dashed lines were taken with two different setups (circuits built on breadboard and with "flying wires") showing the sensitivity of the measurements to stray reactances. The green-shaded region indicates the $\pm 1\sigma$ uncertainty as calculated from the scattered single points (triangles and circles). The red continuous line indicates the calculated ideal transformation ratio.

setup with very short leads (triangle-shaped data-points). Unless the divider is recalibrated for each new PCB, capacitor and leads length used, an overall 20% uncertainty should be considered, especially at the highest frequencies. During the test in liquid helium no significant differences were observed, proving the stability of the mica capacitors at low temperature.
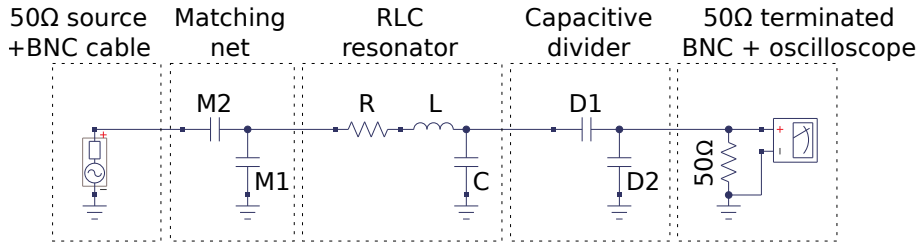
Figure 4.5: Circuit schematic of the first resonator. Components' values are $L = 12\,\mu\mathrm{H}$, $C = 5\,\mathrm{pF}$, $D1 = 5\,\mathrm{pF}$, $D2 = 1\,\mathrm{nF}$, $M1 = 220\,\mathrm{pF}$, $M2 = 900\,\mathrm{pF}$. R can be calculated from the maximum gain: $R = 17\,\Omega$.

4.3. Preliminary testing boards

The first bench testings were done with the use of breadboards, prototyping boards and flying wires. The results were quite unsatisfactory and unpredictable, because of parasitic reactances (boards) and mechanical instability (flying wires). Since then, all the other tests were done on PCBs. The first of these was a PCB drawn by M. Kumph. It is shown schematically in Fig. 4.5 and the PCB itself is shown in Fig. 4.6. It was already available in our laboratory and so it was a fast way to test the resonator, even if some small adjustments were necessary.

4.3.1. Room temperature testing

The first inductor used was an *API Delevan* 5022-123J (Sec. 3.2.3), inductance $12\,\mu\mathrm{H}$. This was chosen, among all the inductors available in the laboratory, because it was the one with the highest $L \cdot Q_{\mathrm{L}}$ product. The manufacturer specifies a component quality factor $Q_{\mathrm{L}} = 65@2.5\,\mathrm{MHz}$ and a SRF at $42\,\mathrm{MHz}$. Using the capacitive divider and a $5\,\mathrm{pF}$ capacitor to simulate the load of the trap, the total capacitance was about $10\,\mathrm{pF}$, from which the resonance frequency should be $\omega_0 = 2\pi \cdot 15\,\mathrm{MHz}$. This frequency is quite high for being useful with the trap Yedikule-1, since at $15\,\mathrm{MHz}$ the desired voltage is very close to the breakdown voltage. If frequency were the main concern, some extra capacitors should be added to lower it. However, since in the near future the plans are to use smaller traps - with lower voltages at higher frequencies - this first test was done at $\omega_0 = 2\pi \cdot 15\,\mathrm{MHz}$ anyway.

The expected gain, calculated from the datasheet through Eq. 3.2.5, was $G_{\mathrm{V}} = 36$. Without the matching, the resonance frequency was $13.11\,\mathrm{MHz}$ and the voltage gain was $G_{\mathrm{V}} = 32$. The 10% error in the resonance frequency is consistent with the error in the
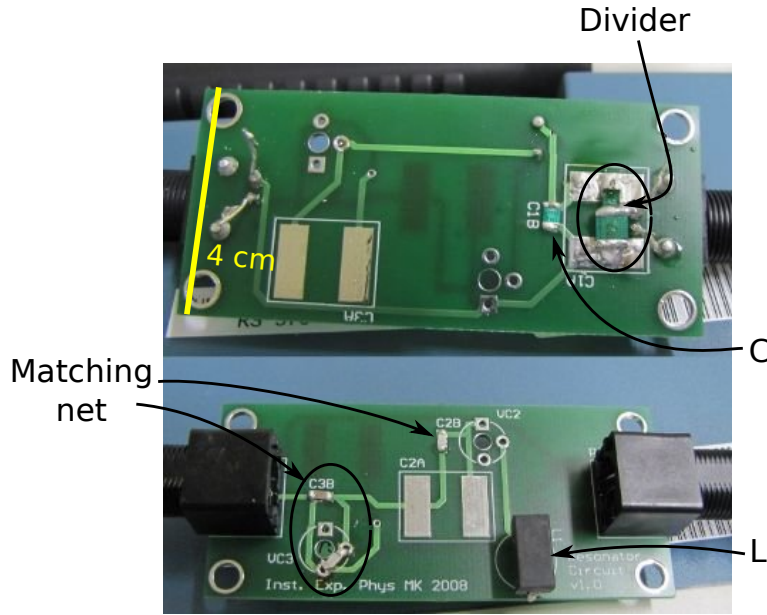
Figure 4.6: Bottom and top layer of the first PCB. This board was used to test the feasibility of a lumped component resonator.

component specifications. The matching circuit, which for this PCB was supposed to be an L-section with two capacitors (region 2 of Fig. 2.12, i.e. frequencies higher than ω_{H} in Tab. 3), was calculated after measuring, with a network analyzer, the impedance of the unmatched resonator. The chosen capacitors were 220 pF (parallel) and 900 pF (series). It should be noted that this type of matching circuit does not provide any DC-path to ground for the resonator's capacitor (and eventually for the ion-trap) which could charge up and provide an unwanted DC offset in the driving voltage. This was, indeed, a defect in the schematic of this PCB: it was acceptable for a quick feasibility testing, but should be avoided in resonators used in the actual experiment.

After the matching, the resonator's resonance was at 13.24 MHz, the gain was $G_{\mathrm{V}} = 34$ and the quality factor, measured from the voltage output, was $Q = 54$. The reflection coefficient was $|S| = 0.004$. From these results it is also possible to calculate the value of the effective resistance ($R = 20\,\Omega$) and the resonator's theoretical quality factor ($Q = 55$). The small difference between the resonator's quality factor and the inductor's quality factor can be explained with $3\,\Omega$ of extra effective resistance, coming from the soldering, the PCB tracks and the capacitors' losses. These results were satisfactory, because the matching was very well done and the voltage gain was almost as high
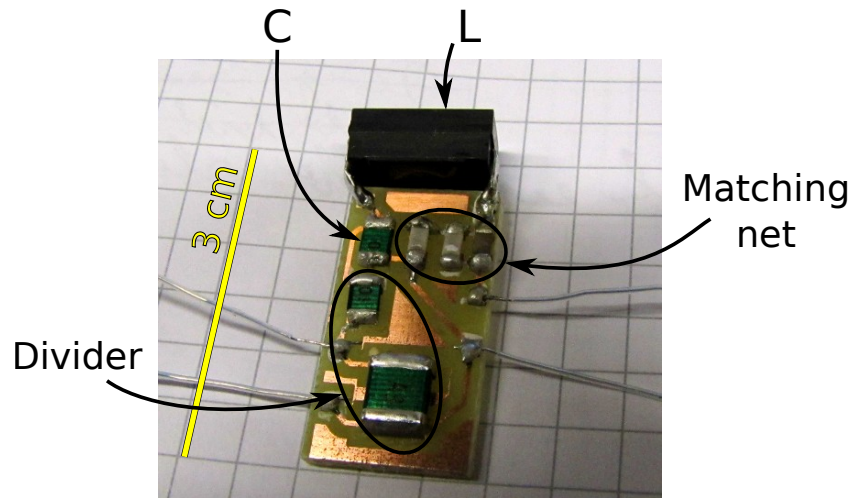
Figure 4.7: The first PCB built for the cryogenic testing, codename *Buggy*. The schematic is the same as in Fig. 4.5. Particular attention was put on the board size: the whole circuit fits in a box of only $2.5\,\text{cm}^3$.

as the maximum obtainable. Nevertheless, this resonator needs to be driven with an amplified function generator ($24\,\text{V}$ peak-to-peak amplitude, $1.44\,\text{W}$ of power) if used to drive Yedikule-1. Despite the promising obtained results, it was impossible to test this circuit at low temperature: the board was too big to be placed into the cryostat's inner shielding.

4.4. Buggy

In order to test the same resonator at cryogenic temperature, a new PCB was drawn and etched. Dimensions were the main focus for this first "home-made" board, which at the end, with all the components mounted, fits in a box of only $2.5\,\text{cm}^3$. The complete circuit looks like a small bug (Fig. 4.7); for this reason its codename was chosen to be *Buggy*.

4.4.1. Room temperature testing

The circuit schematic is again the one shown in Fig. 4.5, exactly the same as in the previous PCB (see Sec. 4.3). Nevertheless, since the matching network is very sensitive to impedance changes, the old values for $M1$ and $M2$ did not work with this new board.

The same matching procedure was then followed again and the two new capacitances were calculated as $M1 = 100\,\mathrm{pF}$ and $M2 = 320\,\mathrm{pF}$. With this circuit, the network analyzer measured a resonance at 13.71 MHz and a scattering parameter $|S| = 0.06$. It is important to stress that, to calculate the matching network, a very precise measurement of the circuit's impedance is necessary. Every unattended impedance, arising from lossy connections or from the coupling between cables or PCB tracks, can change completely the values of reactances necessary for the network.

After the matching, Buggy was tested - at room temperature - inside the cryostat. The RF signal came from a signal generator set to the maximum output amplitude ($10\,\mathrm{V}$ peak-to-peak on a $50\,\Omega$ load). This voltage was amplified by the resonator, and was measured after the divider and the BNC cable with an oscilloscope. The resonance peak was shifted upwards by $0.09\,\mathrm{MHz}$, evidence for a weak coupling between the resonator (probably the inductor) and the cryostat's shielding. The voltage gain, as calculated with this setup, was only $G_V = 17$. This value was significantly lower then the one obtained with the big PCB. To understand better this difference, a probe was then used to measure the voltages at the resonator's input and directly after the capacitive divider[4]. In particular, the latter showed a significant difference between the value right after the divider, inside the chamber, and at the output of the BNC cable, outside the chamber. The voltage at the input of the coaxial cable was $1.18\,\mathrm{Vpp}$, but only $0.82\,\mathrm{Vpp}$ after it. This attenuation of $3.2\,\mathrm{dB}$ is consistent with the expected loss due to the DC resistance of the coaxial line, which was about $16\,\Omega$. It would thus appear that the losses are similar at both DC and RF frequencies. Consequently, considering the real voltage measured inside the chamber, the amplifier's gain was thus $G_V = 24$. The difference between this value and the gain measured with the big PCB can not be explained by the error induced by the calibration of the divider. This means that the limited gain arises from an increased effective resistance due to losses in the coupling between the circuit and the metals (copper) inside the cryostat and also in the coupling between resonator and transmission lines. As evidence for this, we observed crosstalk with amplitude $136\,\mathrm{mVpp}$ on some lines - not directly connected to the circuit - when the resonator was being operated. Unfortunately, these couplings and losses can not be easily predicted, and can only be avoided after various direct trial-and-error tests.

---

[4]As explained, it is not possible to measure directly the amplified voltage, even with the use of a $10\times$ attenuation probe. The extra loading, imposed by the instrumentation, alters the measurement significantly.

4.4.2. Cryogenic testing

The main difference between bench and cryogenic testing is the ability to access the circuit directly. In the first case, the matching network can always be tuned in order to obtain optimal results. In the latter the tuning is not possible because the circuit is inside the vacuum chamber. The picture in Fig. 4.1 was taken immediately before the low-temperature testing of the capacitive divider and the resonator Buggy. After cooling, when no RF power was being used, the minimum temperature reached was $6.8\,\mathrm{K}$. Switching on the signal generator ($250\,\mathrm{mW}$) the temperature rose to $7.6\,\mathrm{K}$. During this heating, the peak-to-peak amplitude of the signal at the capacitive divider was seen to decrease from $1.2\,\mathrm{Vpp}$ to $0.93\,\mathrm{Vpp}$, which means a voltage gain changing from $G_V = 36$ to $G_V = 28$. The resonant frequency was stable at $14.00\,\mathrm{MHz}$, showing a weak dependence on the temperature when compared to the room temperature test. In contrast to the room temperature testing, where the resonator's matching was measured to be $|S| = 0.06$, at low temperature the change in the resonator impedance led to a rise in the scattering parameter to $|S| = 0.14$. This testing demonstrated the feasibility of a low-temperature resonator, moreover improved by the reduced resistance. At the same time, however, it pointed out the difficulty in finding a matching circuit which could be prepared at room temperature to work properly at cryogenic temperature.

4.5. Shy

A new printed circuit board, featuring the resonator and the tracks for the DC trap-electrodes, was developed, etched and tested. In this new design some attempts were made to fix the errors of the previous boards, i.e. including a DC-path to ground and increasing the low gain. The DC-path to ground was provided by simply changing the type of RLC circuit, from series to parallel resonator. To try to increase the voltage gain, a new inductor, with higher Q_L, was used. The name of *Shy* was chosen for this board in reference to a design flaw in the bond pads. This is discussed in more detail later.

Micrometals, Inc. is a company specializing in the realization of ferromagnetic cores for high-Q RF inductors. In one of their application notes [45], they claim that the use of iron powder (micrometer-sized droplet of carbonyl iron) instead of laminated ferrite as the core material, significantly enhances the quality of the inductors. They sell toroidal cores of various sizes and materials and provide software to predict, for each core, the frequency that maximizes the Q_L. The quality factor is influenced by the wire resistivity and diameter, so that to know exactly the maximum obtainable Q_L the fastest way is to test the inductor directly. Using *Micrometals*' software and their iron-powder core a
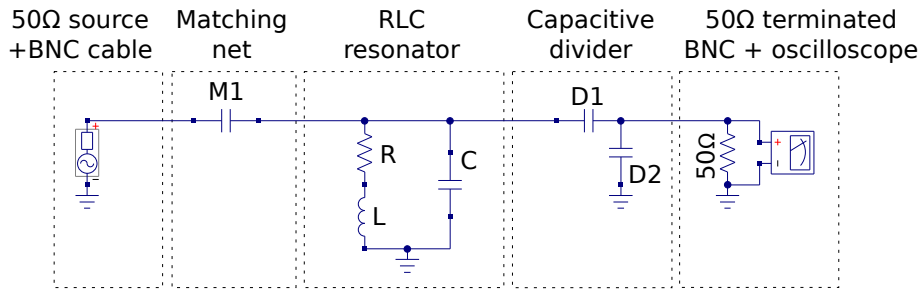
Figure 4.8: Shy's schematic. It is a parallel RLC circuit, with a capacitive divider and a matching network made with only one capacitor. The values used are $L = 10\,\mu\text{H}$, $R = 10\,\Omega$, $C = D1 = 5\,\text{pF}$, $D2 = 1\,\text{nF}$, $M1 \simeq 8\,\text{pF}$.

new inductor of approximately $12\,\mu\text{H}$ - the same as the *API Delevan*'s SMD inductor already tested - was designed and built. This inductor was measured with a spare resonator PCB: the inductance value was estimated, from the resonance peak, to be $10\,\mu\text{H}$, while the effective series resistance was estimated, from the unmatched input voltage on resonance, to be $10\,\Omega$.

4.5.1. Room temperature testing

The new PCB was built and the components soldered. The schematic and the physical circuit are shown in Fig. 4.8 and in Fig. 4.9, respectively. The differences between this board with the first one are

- RLC resonator type changed from series to parallel;

- bonding pads included;

- matching network composed of only one variable capacitor;

- RF coaxial cable connected directly to the board.

The matching circuit was chosen to be made with only one capacitor for simplicity, as explained in Sec. 3.3. In order to match the high impedance of a parallel resonator near resonance, the necessary capacitance is small ($< 10\,\text{pF}$). In addition, since in this case the matching is much more sensitive to the value of this capacitance, the use of a variable capacitor was the easiest solution. The coaxial cable carrying the RF signal was connected directly to the board as an attempt to reduce the crosstalk between different
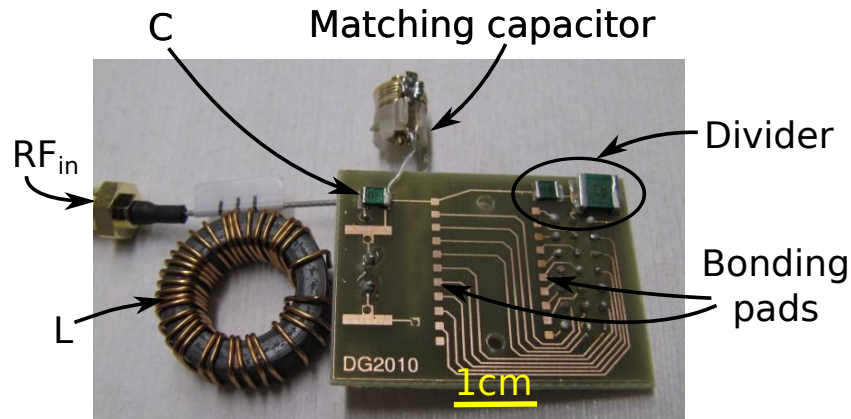
Figure 4.9: The parallel RLC resonator, codename *Shy*. The new toroidal inductor, L, is visible on the left of the picture. The *Samtec* micro coaxial cable, RF_{in}, also on the left, is used to feed the RF signal. The matching is done with only one series capacitor, on the top border. The pads for the bonding with the trap electrodes are placed at the center of the PCB and are connected to the pogo-pins counter connectors.

lines. *Samtec* manufactures both the small, flexible cable (product series MH081) and the miniaturized SMD connectors (RSP-122893-02).

The experimental testing of this board matched exactly the expected results obtained with an open-source circuit-simulator software called *Qucs*[5].The resonance peak was at 12.00 MHz, and the voltage gain was $G_V = 34$. With the gain higher than before, and the resonance peak at a lower frequency, it was in principle possible to trap with 1 W of input power from an amplified signal generator. The desired limit of 250 mW was not satisfied, but this resonator was prepared to be bonded to the trap anyway. Unfortunately, with the ultrasonic wire bonder available in the cleanroom, it was impossible to reach the pads, which were too close to the trap carrier and too deep with respect to the trap plane. The codename *Shy* for this board was chosen for this reason. Since it was impossible to build the complete circuit, with the trap and the gold wires, the cryogenic temperature testing was skipped and another board was drawn to fix the problem.

---

[5]Quite Universal Circuit Simulator, http://qucs.sourceforge.net. This is an open-source circuit simulator founded by M. Margraf. As stated on the website "The software aims to support all kinds of circuit simulation types, e.g. DC, AC, S-parameter, Harmonic Balance analysis, noise analysis, etc.".
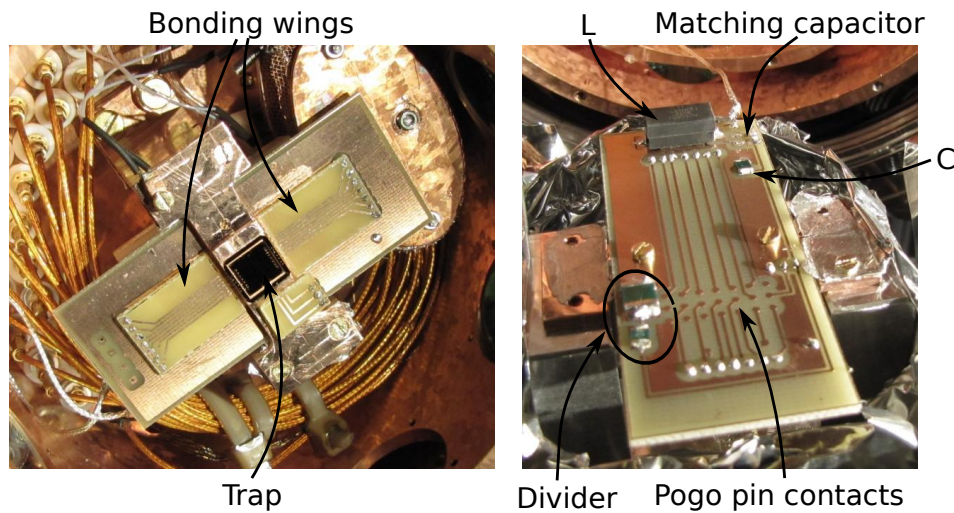
Figure 4.10: *Wingy* is the resonator used to drive for the first time the trap Yedikule-1. In the pictures both the top and the bottom layer are visible. Characteristic of this board is the presence of three small PCB pieces used to interface the real resonator's PCB and the bonding wires.

4.6. Wingy

Shy's design flaw was solved applying two large PCB-wings on the trap side, in order to provide higher and wider pads to bond the gold micro-wires (see Fig. 4.10). From this added boards, the codename *Wingy* was chosen for the new resonator. The fabrication process of this circuit was more complicated than the other PCBs shown so far, but at least in this way the bonding was possible.

4.6.1. Room temperature testing

During bench testing (outside the cryostat) of the board, the resonance peak was at 10.3 MHz and the voltage gain was $G_V = 30$. The problems of this board arose during the testing inside the cryostat. The first problem was a sudden drop in the gain when the resonator was placed into the cryostat. An analysis done with a simulation of the resonator showed that the matching capacitor which maximizes the voltage gain (5 pF) is different from the capacitor which minimizes the scattering parameter (8 pF). The resonator showed, indeed a very high scattering parameter $|S| = 0.85$. After some trial-and-error test on Wingy, the best matching capacitor was found to be 10 pF, but the gain

was still as low as $G_V = 6$. A possible source of losses could be the coupling between the resonator and the copper parts or the other signal lines, as happened with Buggy. With this board, were the etched tracks were longer than in the previous designs, the coupling is expected to be higher. Two different versions of this board, with different layouts, were tested to try to reduce the coupling, without much success. In an attempt to reduce the coupling, the shielded SMD inductor was used again instead of the toroidal one. The only result was a lower resonance frequency (8.3 MHz), but still a comparable voltage gain. By contrast, the Q factor was still high, approximately $Q = 33$ when measured from the voltage bandwidth. This resonator was tested also at low temperature, though it was never used to trap ions.

4.6.2. Cryogenic testing

Wingy gave poor results at room temperature, which did not get better at cryogenic temperature. The resonance frequency, the gain and the quality factor were roughly the same in both testing, but additionally some more difficulties arose:

- in the first version of the PCB, a short between the amplified RF track and the trap carrier - held at ground - happened at low temperature. The two lines were close to each other, and when the fastening screws shrunk because of the thermal contractions, the track and the copper part touched each other. This problem was partially solved using several layers of kapton foil for electrical insulation and was completely eliminated in the second PCB design;

- the signal was unstable, and sometimes completely missing. In a similar manner to the problem above the PCB deformations, due to unbalanced stresses on the board, created loose connections with some pogo pins. A small aluminum bar, shaped as a horseshoe, was fixed to the trap mount underneath the PCB, in order to provide mechanical support. Despite this attempt, the signal problem was still present in the successive cool down cycles;

- with the toroidal inductor multiple resonance peaks, at 10, 15, 18 and 24 MHz, were observed. The reason for this behavior is not completely understood, but it can be that the internal structure of the ferromagnetic domains changed after the first cool down. This error remained at room temperature, too, after the heat-up of the cryostat.

Despite various attempts to improve the gain, this resonator never satisfied the constraints given. In the development of the next resonators, Airy and then SCairy, all the

problems encountered with Wingy were kept in consideration and most of them were solved.

4.7. Airy and SCairy

Because of the unsatisfactory performance of the previous board, Wingy, especially during the cryogenic testing, the series RLC scheme was preferred for the subsequent resonator. In addition, in order to avoid any side-effects given by the ferromagnetic core at low temperature, the inductors used were manually wound without any core or onto small plastic tubes, used just as a mechanical supports. From these air-core inductors, the resonator's codename *Airy* was taken.

4.7.1. Room temperature testing

The new circuit, first tested with M. Kumph's big PCB, is essentially the same as in Fig. 4.5, with M1 being an inductor instead of a capacitor. To provide a DC-path to ground for the trap using a series resonator, the matching was done with one parallel inductor instead of a parallel capacitor. In addition, a capacitor was added in series with the circuit to fine-tune the matching. The capacitance had to be big (small impedance) because most of the matching was done with the inductor. Using a variable ceramic capacitor the search for the perfect matching was much easier and faster, but the highest capacitance available for small-sized variable ceramic capacitors is only $100\,\mathrm{pF}$.

The inductors were calculated using an RF inductance calculator available on-line[6]. This software has various valuable features: it includes in the calculations the stray capacitive coupling between windings, skin effect and proximity effect. Given the diameter of the windings and of the wire, the number of turns and the length of the coil, it can calculate the inductance, the self-resonance frequency and the quality factor Q_{L} for a given frequency. Compared to the inductance calculation formula usually reported in handbooks [39]

$$L = \frac{N^2 r}{22.9 + 25.4 l/r} \cdot 10^{-4}\,\mathrm{H/m} \tag{4.7.1}$$

(N being the number of windings, l the coil length and r the coil radius) this simulator offered much more accurate results. As an example, the error in the inductance of the main inductor used for Airy was only 10%, most of which due to the uncertainty in the diameter. With Eq. 4.7.1 the error was slightly smaller than 20%.

---

[6] http://hamwaves.com/antennas/inductance.html

With reference to Fig. 4.5, the circuit was built with the following components: $L = 6.8\,\mu$H, $C = D1 = 5\,$pF, $D2 = 1\,$nF, $M1 = 250\,$nH, $M2 = 100\,$pF (variable). The matching ($|S| = 0.00$, less then the network analyzer resolution) was achieved just by turning the variable capacitor and monitoring the scattering parameter in real-time with a network analyzer. The characterization of the resonator gave a resonance frequency at 18.9 MHz, a voltage gain $G_V = 43$ and a quality factor $Q = 130$ (from the voltage bandwidth) or $Q = 125$ (from the scattering bandwidth). The calculated equivalent resistance was thus $R = 5.6\,\Omega$.

This resonator did not meet the given requirements to work with Yedikule-1, but it was inspiring for the successive developments because

- it showed the possibility to build high-quality air-core inductors

- it opened the possibility to wind coils with different wire materials

- winding any specific inductor is faster than ordering them from distributors

- changing the coil length it is possible to increase the inductance without drastically reducing the self-resonant frequency

The drawback of using air core solenoids are the coil dimensions, which are bigger than coils with ferromagnetic cores; as an example, an inductance of $40\,\mu$H, with a SRF higher than 20 MHz, should be at least $10 \times 10 \times 20\,$mm^3.

In order to build a resonator which could meet the requirements for Yedikule-1, two different ways were possible. The first was lowering the resonant (and so the working) frequency till a maximum of 9 MHz. Given a gain comparable to the one obtained with Airy, at this frequency the minimum stable-trapping voltage (200 V) could be reached without any power amplifier. The second way was improving the voltage gain: as stated in Sec. 3.2.3, this can be done with bigger inductances and bigger quality factors. In Fig. 4.11 the newest (and last) resonator is shown. The resonant frequency was lowered using a bigger inductance $L = 36\,\mu$H (dimensions $20 \times 20 \times 20\,$mm^3) and a superconducting cable was used in the attempt to improve the quality factor when the critical temperature was reached. The cable is manifactured by *Supercon Inc.*; it is made of NbTi (Niobium Titanium), stabilized with copper. The superconducting critical temperature is 9.2 K, above the usual minimum working temperature of the cryostat of this experiment (7 K). The cable is a Litz wire[7] made with 54 superconducting filaments, with a final insulated diameter of only 0.279 mm.

---

[7]Litz wires are usually preferred in AC application because their resistivity is less affected by the skin effect.
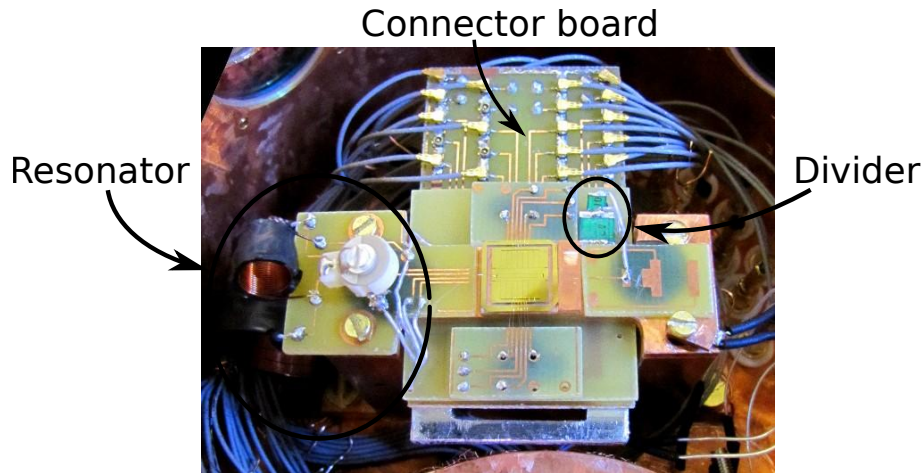
Figure 4.11: The last PCB built, *SCairy*, is composed of four boards plus a connector board for the pogo pins. The lateral "wings" are shorter than in Wingy in order to have a long and narrow board which could eventually fit into the liquid helium dewar. The resonator size is about $10\,\mathrm{cm}^3$, as prescribed in Sec. 2.2.

This new resonator, being the superconducting analogue of Airy, was called *SCairy*. It was tested at room temperature and at cryogenic temperature. When tested outside the cryostat, without a connected trap, the resonator showed a resonance frequency at 8.14 MHz, the gain was $G_V = 55$ and the quality factor was $Q = 80$. When tested inside the cryostat, with Yedikule-1 mounted and bonded, the resonant frequency was lower, $\omega_0 = 2\pi \cdot 7.43\,\mathrm{MHz}$, which could be explained with a trap capacitance of $C_{\mathrm{trap}} = 2\,\mathrm{pF}$ (a capacitance bigger than the expected $1\,\mathrm{pF}$). The gain and the quality factor were lower, too, being $G_V = 46$ and $Q = 62$. Looking at these parameters, this resonator seemed to be the first to satisfy the requirements given in Sec. 2.2. The last two requirements - i.e. the cryogenic and the vacuum compatibility - were then tested and the results are reported in the next subsection.

4.7.2. Cryogenic testing

As stated, SCairy had a resonance frequency and a voltage gain high enough to trap with very low input power. The only requirements still to check were the vacuum compatibility and the cryogenic compatibility. The requirement of vacuum compatibility is not stringent at low temperature, and it is hard to check with the actual setup. The

minimum pressure reached in the outer chamber, when the resonator where in vacuum and the cryostat was running, was on the order of 10^{-8} mbar, which is the same pressure reached when no resonator was present. Thus, it is safe to say that the board does not outgas significantly more than the rest of the equipment in the chamber, within this resolution. Till now this test was sufficient, because the trap was always operated at cryogenic temperature where the vacuum compatibility is not a problem. When room temperature trapping will have to be achieved, a better compatibility test should be performed. This can be done placing the circuit in a different chamber, possibly equipped with an RGA (mass spectrometer). After a long bake-out the final pressure can be measured thus proving (or rejecting) the UHV compatibility.

For the cryogenic compatibility, the temperature was measured on the copper of the trap carrier and in the charcoal of the cryo-pump. The two measurements agreed within 0.5 K, and it is reasonable to assume that the cables were at the same temperature. Both the gain and the quality factor (determined from the voltage bandwidth) were measured as a function of the temperature. The results are reported in Fig. 4.12. The two plots increase with decreasing temperature, showing an improvement of the resonator at low temperature. At the minimum temperature reached, $T = 5.7$ K, the quality factor was $Q = 720$, more than one order of magnitude higher than at room temperature. In a similar way, the gain was $G_V = 100$, more than twice the gain in the beginning. It is interesting to observe the diminished gain at 7 and at 6 K, and an increased Q at the same temperature. The reason for this behavior is not clear, but probably the most reliable value is Q, since the quality measurement is independent of voltage scale factors. By contrast, the maximum gain is proportional to the amplitude of the RF wave at resonance, which could be diminished with loose contacts.

The quality factor exhibits a big change around the superconducting-transition temperature of the niobium cable used to wind the two coils. The finite value of Q is an evidence that some effective resistance is always present: it could be due to the contact-resistance, the resistance of the PCB tracks or even the losses in the capacitors. In any event, since the resistance of the coils was not measured, it is not known if the inductors were superconductive or not.

The resonance frequency showed a negligible change, moving from 7.43 MHz at 300 K to 7.645 MHz at 5.7 K. The scattering parameter S changed from 0.027 to 0.57. This is due to the small effective resistance, which at low temperature is 10 times lower than at room temperature. The matching, which was achieved at 300 K, is no longer good at 5 K. If necessary, the matching can be done at low temperature, repeatedly immersing the resonator in a liquid helium dewar and then tuning the matching capacitor. With this procedure in mind, the PCB was drawn to be small enough to fit in the neck of the dewar (4 cm). This matching should be done with a dummy trap connected, in order
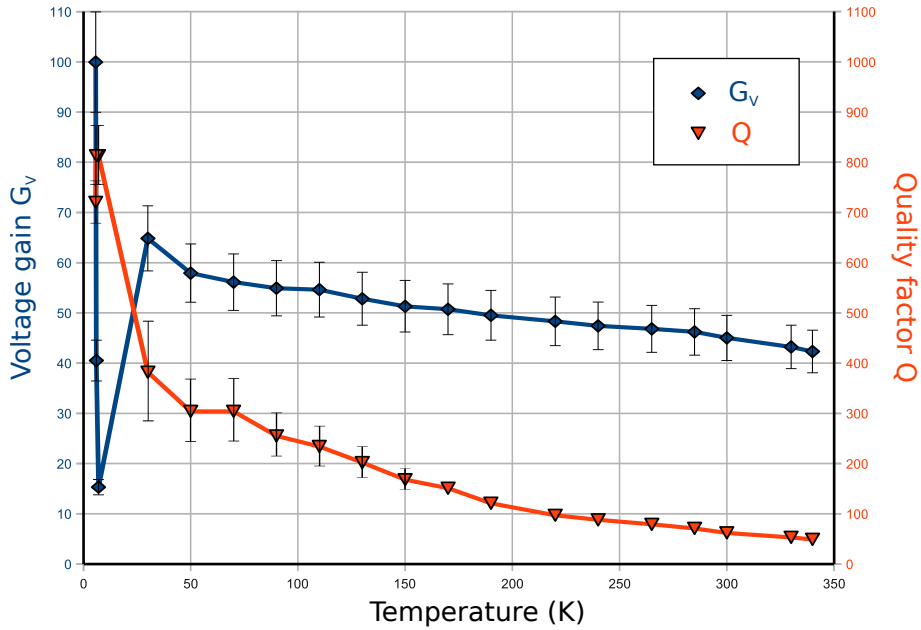
Figure 4.12: Temperature dependence of SCairy's voltage gain and quality factor Q. The lines connecting the datapoints are drawn as a guide to the eye. The error bars on the voltage gain come from the systematic error of the calibration of the capacitive divider. The calculated error bars on the quality factor are due to the instrumental uncertainty in the frequency measurement.

to not damage the real trap. For the time being, since the voltage gain is high enough and the function generator is not damaged by the reflected power, this procedure is not necessary. This resonator was used to successfully trap ions. It should be noted that this is the first time that a superconducting lumped-components resonator is used in this field.

4.8. Summary

Following this long list of resonators, with features and problems encountered for each of them, it is opportune to summarize the important results. This is done in Tab. 4. From Sec. 2.2 it may be noted that the requirements for a resonator for use in the present ion trapping system are fully satisfied only by SCairy.

Name	Design features	Room temperature test			Cryogenic temperature test			Problems
		$\omega_0/2\pi$ (MHz)	G_V	Q	$\omega_0/2\pi$ (MHz)	G_V	Q	
(preliminary test)	Good matching with two capacitors	13.24	34	54	-	-	-	Too big for the cryostat
Buggy	Small board dimensions	13.80	24	-	14	28	-	No connections with the trap, no DC path to ground
Shy	Parallel RLC, DC-rejection, iron-powder-core inductor	12.00	34	-	-	-	-	Trap bonding not possible
Wingy	Wide bonding pads	8.3	6	33	8.3	6	-	Multiple resonances, low gain, instability
Airy	Air-core inductor, series RLC, easy DC-rejecting matching	18.9	43	130	-	-	-	Low gain (for the given frequency)
SCairy	Superconducting air-core inductor, lower frequency	7.43	46	62	7.645	100	720	Difficult matching at low temperature

Table 4: Summary of the important results, features and faults of the tested resonators.

5. Improvements and outlook

The feasibility of a small voltage amplifier to be used to drive the RF electric field of a cryogenic ion-trap is now proven. The physical realization of such a device additionally showed the advantages and the critical points of using an RLC circuit to reach the goal. During the development process, various new features were added and some design faults were fixed, but it is still possible to do something to improve the trap-drive circuit. Here some ideas are reported and critically analyzed.

5.1. Superconducting resonator

Dissipations are the bottle neck which limit the gain and the quality of a resonator. The use of superconducting cables to wind air-core inductors showed, with SCairy, that enhanced gains are obtainable at low temperature. This opens the possibility to operate at higher frequencies, where high voltages are difficult to obtain (using low-power sources). Resonators built completely with superconducting materials are possible, but their main use is for passive filtering. On the topic numerous articles are available in literature, among them [46, 47, 48]. One of the most used superconducting material is YBCO, because of its high critical temperature, which enables the use of liquid nitrogen for the cooling. In the last decade many improvements were done in the area of YBCO film deposition on different substrates, and the patterning of circuit elements, like inductors or capacitors, is now possible.

Designing a pattern including both the resonator and the trap enables the possibility to reduce many sources of dissipation. An indicative schematic is shown in Fig. 5.1. For the best results the capacitive divider should be omitted, in order to not overload
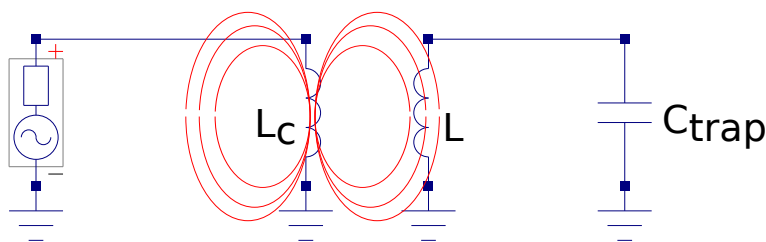

Figure 5.1: Suggested scheme for a superconducting resonator. If $L_C \ll L$ a step-up voltage transformation is achieved in the coil on the right. By varying the spacing of the inductors it is possible to adjust the coupling (red lines) and maximize the gain.

the circuit, and the gain should be determined by the quality factor measured from the S-bandwidth[8]. The coupling could be done inductively, and the coupling strength varied to fine-adjust the matching. On the left hand side, the condition $L_C \ll L$ should be met to provide a considerable step-up in the voltage in the resonator. The capacitance should be given by the trap only, so that bigger inductances can be used in the resonator for a given frequency.

With the actual technologies available in our cleanroom, the fabrication process of superconducting films with critical temperature above $10\,\mathrm{K}$ is not doable. However, in the perspective of scalable ion-traps, this possibility should be taken into account, as it would provide higher gains, smaller dimensions and a better integrated system (trap and resonator on the same chip).

5.2. Tunable circuit

One significant limitation encountered during this project was the impossibility of acting on the circuit when the resonator was in vacuum. In a "tunable circuit" it should be possible to easily change the impedances in order to tune both the matching and the resonance frequency. In Sec. 2.4, the importance of a good matching network was already pointed out. In addition, the big changes in the scattering parameter S, between room and cryogenic temperatures, were shown in chapter 4. It is thus obvious why the possibility of tuning the matching of the circuit in real-time is beneficial.

Tuning the frequency is not important if the goal of the experiment is just to trap ions and do quantum operations. However, it could be useful in the systematic study of anomalous heating, where the dependence of the noise power spectrum to the trap RF frequency is still to be investigated. Heating rates for the same single ion, in the same environment, could be measured while scanning the frequency in real-time. In the following, three different ideas on how to obtain the desired tuning are suggested.

5.2.1. Mechanical tuning

Of course, the most obvious and easy way to change the impedances is by means of ready-made, standard variable capacitors and variable inductors. These are simple passive elements, where the reactance is changed by turning a knob. One of these variable capacitors was used with great success in Airy and SCairy, making the matching process much faster. Accessing the knob in vacuum, however, requires some sort of mechanical feedtrough, either linear or — better — rotary. Moreover, the bar connecting the knob

---

[8]The value of the inductance or the capacitance should be quite reproducible using this procedure of patterning-deposition.
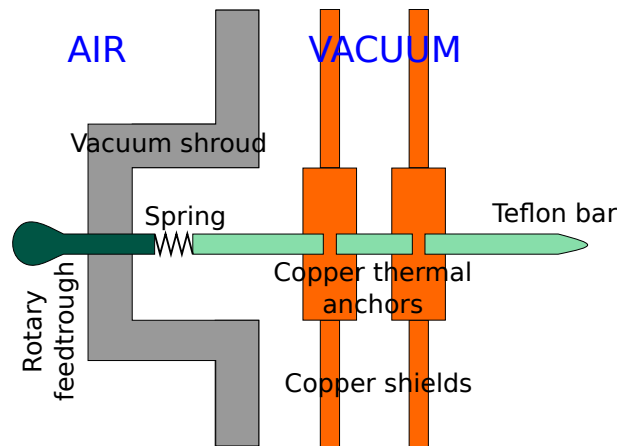
Figure 5.2: Cutaway sketch of a mechanical tuning apparatus. The Teflon bar is divided in three different pieces, connected by two copper disks, which are in thermal contact with the copper shields. A spring connecting the Teflon bar to the rotary feedtrough could compensate for thermal contractions in the bar.

to the mechanical feedtrough will be short (roughly 10 cm) and exposed to a large temperature gradient (from 300 K to 5 K). To limit the transport of heat into the inner shield of the cryostat, thermally insulating materials such as Teflon should be used. A nice trick to reduce the thermal load on the resonator and the trap could be the use two small pieces of copper, placed on the bar in proximity to the copper shields, thus anchoring the temperature of the stick to the temperature of the shield (Fig. 5.2). This type of mechanical actuator seems both simple and feasible. However, its implementation will require significant changes in the actual setup.

5.2.2. Electrical tuning

An alternative to the mechanical feedtrough could be an all-electrical tuning with the use of varicap diodes. These diodes are meant to be operated in reverse-bias, so that no current can flow. Changing the biasing voltage, the thickness of the depletion zone vary and the capacitance changes accordingly, ideally as the inverse square root of the biasing voltage. The idea, thus, is to use these varicap diodes instead of the variable capacitors, both in the matching network and in the resonator's capacitance, and then tune them via DC voltages (see Fig. 5.3).

One challenge in this system is how to bias the diodes which have relatively-high RF signals crossing them. At the matching diode, for example, the RF amplitude is at least
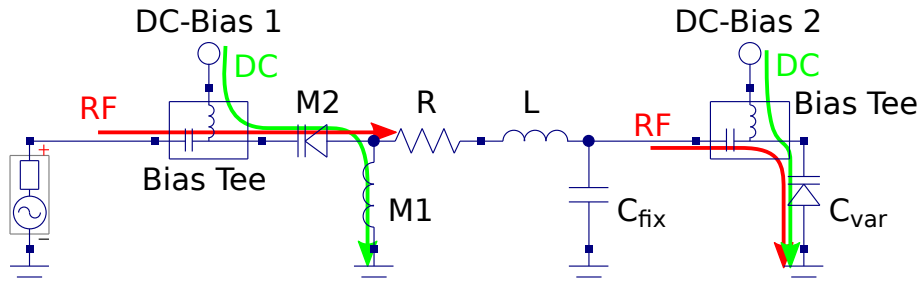
Figure 5.3: Schematic showing the resonator tuned via varicap diodes. Two bias-tee are used to control the diodes without biasing the RF voltage in the resonator or in the function generator. The red and green line are the ideal path followed by the RF and DC signal, respectively.

1.5 V (for SCairy, driving Yedikule-1 at 5.7 K). A biasing voltage, to be robust enough, should be ~ 10 times bigger (i.e. 15 V or more). At these voltages, the available varicap diodes have capacitances in the range of 10 pF, while for a reasonable matching range this value should be ~ 10 times bigger, requiring for an array of at least 10 parallel varicap diodes.

In the resonator, the problem is even more serious: first of all the quality factor of varicap diodes is of order 100, thus limiting the best Q achievable by the resonator. Secondly, the RF amplitudes are of order 150 V. It is thus necessary to reduce the RF voltage across the diode using another small capacitor placed in series, acting like a capacitive divider. The smallest mica capacitor available is 1 pF. Now, when the bias is high (30 V typically), the capacitance of the diode is low (10 pF) and the divider ratio is 10, so that the maximum RF amplitude across the divider should be $10 \times 30/10 = 30$ V. When the bias is low (2 V) the capacitance is high (100 pF) and the maximum RF amplitude at the divider input should be $100 \times 2/10 = 20$ V. In both cases, something like 10 dividers must be placed in series, distributing the high resonator RF amplitude equally. It is easy to see that the total tuning capacitance ranges from about 0.09 pF to 0.1 pF, thus changing the total resonator capacitance by only 2% (assuming that only the trap capacitance is present) and the resonant frequency by only 1%. With an array of 10 tuning rows (100 diodes and 100 mica capacitors!) the total capacitance can be made to vary by 10%, and the frequency by 5%. In this case the result does not pay for the effort spent.

5.2.3. Electro-mechanical tuning

A third option is to merge the good features of both the methods described above. A good tuning circuit should be stable even with high amplitude RF voltages, like the case of the mechanical tuning, and it should be driven electrically without changing too much the actual setup. In the following, two ways to achieve this goal are proposed.

The first proposal involve the use of standard variable capacitors, as proposed for the all-mechanical tuning, tuned by means of electric motors. Since any stray magnetic field could influence the ion Zeeman splitting, and thus the fidelity of coherent operations, these motors have to be non-magnetic. Even if a continuous and stepper motor could be made, in principle, without the use of ferromagnetic parts, it turns out that none of them are available commercially (probably because of the low torque achievable without ferromagnetic cores). Nevertheless, there exist a class of motors which do not need magnetic fields and which can operate at cryogenic temperatures. These are acoustic-wave motors, where the rotor is moved by the repeated contraction and expansion of a piezoelectric material. These actuators are usually very accurate, with sub-nanometer resolution, but they are very expensive, too, with prices sometimes exceeding €10, 000. A reasonable alternative is given by the company *PCBMotor ApS*. Their motor kits cost in the range of a few hundred euro. The driving electronics is very simple and the PCBs can be customized. These motors are small, about $20 \, \text{cm}^3$, but unfortunately not small enough to easily be placed in the cryostat, even when customized. This precludes the use of such actuators in the experiment.

The second proposal uses completely different variable capacitors. The idea is to build two plates and then move them with linear actuators. Again, there exist two classes of linear actuators: the first is the accurate and expensive class of slip-sticks, the second is the class of piezoelectric actuators, either linear or bendable (where the voltage applied cause opposite contractions in two layers of piezoelectric material, thus bending the stack). The limiting factor for these actuators is the displacement at low temperature, which is reduced by a factor of ten with respect to the displacement at room temperature. For reasonable displacements, in order to achieve the desired range of capacitance, the physical dimensions of these actuators are too big for the cryostat, exceeding the value $10 \, \text{cm}^3$ given in Sec. 2.2. Another concern which must borne in mind is the noise that could be produced by the vibrations of these movable plates.

5.3. Summary

In this section some ideas on how to improve the features and the usability of the resonator were outlined. The idea of an all-superconducting resonator was inspired from

the good results obtained with SCairy. However, even with a superconducting resonator, some dissipation will always be present. It is thus not clear what the maximum gain achievable with such a system could be. With our current technology it is not possible to test this, but in the near future it will be worth investigating the possibility offered by superconductors.

The possibility of tuning the circuit is an interesting and desirable feature. However, none of the proposed methods to achieve this task is completely satisfying. The best way, at this time, seems to be the all-mechanical tuning, for its simple design, the small volume occupied (only the Teflon bar comes inside the 4 K shield) and the absence of stray electric or magnetic fields. The cost is limited, too, being around €1,000. Currently a tunable circuit was not necessary, and thus the actual setup was not modified. In the future, if the ability to change the resonance frequency or the matching impedance will become the main concern, this or one of the proposed alternative can be adopted.

6. Conclusions

This thesis describes the basic principles needed to understand and develop a lumped component, passive, radio-frequency voltage amplifier. The circuit was studied to be used to trap calcium ions with a micro-fabricated planar surface linear trap. The theory underlying Paul traps was explained in Sec. 2.1. With this, some requirements for the desired trap-drive circuit were set, bearing in mind the cryogenic environment in which the amplifier should be operated (Sec. 2.2). The operating frequency range (from ~ 7 to $\sim 16\,\mathrm{MHz}$) is set by the trap geometry, the ion mass and the maximum voltage achievable.

Trapping requires high radio-frequency electric fields, whereas the use of a cryostat requires low power consumption. A good way to store energy in the electric field with a minimal use of RF power is exploiting the resonant effect of an RLC circuit. The theory of series RLC resonators was given in Sec. 3.1 together with the analysis of the effect of a matching network. The factor which limits the maximum gain of these resonators, and so the maximum frequency, is the effective series resistance, which at high frequency is almost completely given by the inductor's losses. The value of this resistance is usually reported as a quality factor: the ratio between the absolute reactance and the resistance of the complex impedance (the inductor, in this case). To achieve the best voltage gain possible, it is necessary to maximize the product $Q_\mathrm{L} \times L$, as explained in Sec. 3.2. Unfortunately there are upper limits to both L and Q_L: big inductances cannot be used because of the self-resonance frequency, which makes the inductor to behave like a capacitor, while high quality factors are difficult to reach because of the skin effect and the proximity effect.

With the appropriate choice of the operating frequency, the matching network can be made with only one reactance. A DC path to ground has to be provided to the trap for better stability, thus suggesting the use of a parallel inductor (Sec. 3.3). Nevertheless, since inductors are difficult to tune, an additional series variable capacitor should be used for the fine tuning of the matching. Parallel RLC resonators naturally provide a DC path to ground for the trap, and can be matched with only one capacitor. Even if they seem to be preferable for this reason, the experimental test pointed out some intrinsic difficulties (the matching circuit which maximize the gain and the one which minimize the reflection are different) and showed very poor gain (this second problem probably due to other causes, beside the parallel RLC configuration).

The experimental realization and testing of several resonators (Sec. 4) showed the challenge imposed by the given constraints: a small resonator, with a small inductor, has to be carefully engineered to provide a suitable voltage gain. The best results were obtained with manually-wound air-core inductors, using either copper or niobium-
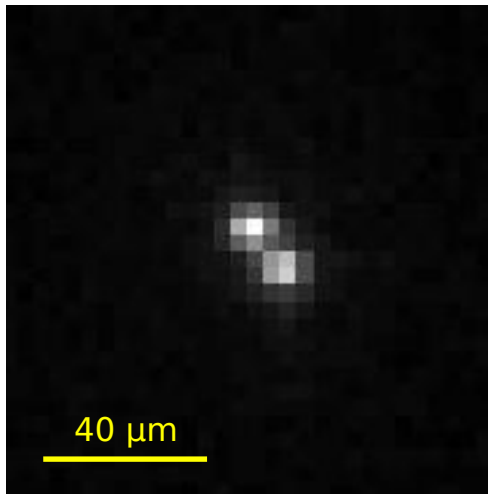
Figure 6.1: The first two $^{40}Ca^+$ ions observed in the cryostat, trapped with Yedikule-1 and the voltage amplifier developed in this thesis, SCairy. The bright spots come from the fluorescence light of the $D_{5/2}-S_{1/2}$ transition ($\lambda = 397\,nm$) used for Doppler cooling. The ion-ion distance is $\sim 20\,\mu m$.

titanium wires. With the superconducting (NbTi) inductor, a high quality factor ($Q = 720$) and a high voltage gain ($G_V = 100$) were observed at low temperature. With this resonator two calcium ions were successfully trapped using only $18\,mW$ of RF power (see Fig. 6.1).

Resonators with high Q (and high gain) are more susceptible to impedance changes and are, therefore, more difficult to be tuned at low temperature. If the tuning of the matching network is done at room temperature, the value of the scattering parameter can easily exceed 0.5 at low temperature. For this reason it is desirable to have a way to tune the circuit in vacuum in real-time. Several proposals for how to accomplish this were given in Sec. 5. Notably, Sec. 5.1 proposed an improvement where an all-superconducting resonator is used: if the resistance of the cables is removed, the only dissipations left come from eddy currents in the materials surrounding (and coupled to) the circuit. Shielding the circuit and limiting these couplings, the voltage gain should be much higher than what was obtained with the resonators built so far.

In conclusion, the possibility to trap ions with a compact RF amplifier made with standard lumped components was proven. The efforts spent to increase the voltage gain enabled, for the first time, trapping of calcium ions with only $18\,mW$ of RF power.

Appendices

A. Matching with one reactance

As in the scheme of Fig. 3.6, let the impedance of the series RLC resonator be

$$Z(\omega) = R + i\left(\omega L - \frac{1}{\omega C}\right) = R + iX(\omega) \tag{A.1}$$

where the definition $X(\omega) := (\omega L - 1/\omega C)$ was used. The relation to be satisfied when matching with only one reactance is

$$\frac{1}{Z_{\mathrm{s}}} = \frac{1}{Z(\omega)} + \frac{1}{iX_{\mathrm{m}}(\omega)} \ . \tag{A.2}$$

Since Z_{s} is real, $iX_{\mathrm{m}}(\omega)$ is imaginary and $Z(\omega)$ is complex, it is possible to split the relation in two different equations to be satisfied:

$$\begin{cases} \mathbb{Re}\left(\frac{1}{Z(\omega)}\right) = \frac{1}{Z_{\mathrm{s}}} \\[2mm] \mathbb{Im}\left(\frac{1}{Z(\omega)}\right) = \frac{1}{X_{\mathrm{m}}(\omega)} \ . \end{cases} \tag{A.3}$$

From the first relation it is easy to find

$$Z_{\mathrm{s}} = \frac{R^2 + X(\omega)^2}{R} \tag{A.4}$$

$$X^2(\omega) = R(Z_{\mathrm{s}} - R) = R^2\alpha \tag{A.5}$$

where $\alpha := Z_{\mathrm{s}}/R - 1$ was defined. A necessary condition for the solution's existence is $Z_{\mathrm{s}} > R$. Solving for X leads to two opposite solutions

$$X(\omega_{\mathrm{H,L}}) = \pm R\sqrt{\alpha} \ . \tag{A.6}$$

The positive solution (inductive behavior) appears at a higher frequency (ω_{H}) than the resonance frequency. The negative solution (capacitive behavior) shows up at a lower frequency (ω_{L}). Substituting with the explicit form of $X(\omega)$ (see Eq. A.1), a second order polynomial has to be solved

$$\omega^2 \mp \omega\frac{\omega_0\sqrt{\alpha}}{Q} - \omega_0^2 = 0 \tag{A.7}$$

where Q and ω_0 are defined as always. Two of the four solutions are negative. The two remaining solutions (positive solutions) are

$$\omega_{\mathrm{L}} = \omega_0\sqrt{1 - \frac{-\alpha}{4Q^2}} - \frac{\omega_0}{2Q}\sqrt{\alpha} \tag{A.8}$$

$$\omega_{\mathrm{H}} = \omega_0\sqrt{1 - \frac{-\alpha}{4Q^2}} + \frac{\omega_0}{2Q}\sqrt{\alpha} \;. \tag{A.9}$$

From $X(\omega_{\mathrm{H,L}})$ it is also easy to find the matching impedance

$$X_{\mathrm{m}}(\omega_{\mathrm{H,L}}) = \mp\frac{Z_{\mathrm{s}}}{\sqrt{\alpha}} \tag{A.10}$$

which confirms the obvious observation that a capacitive behavior can be matched with an inductor, and vice versa. It is interesting to know if matching at a different frequency from the resonance leads to big losses in the voltage gain. To answer this question the transfer function at the two frequencies $\omega_{\mathrm{L,H}}$ must be calculated:

$$G_V(\omega_{\mathrm{L,H}}) = \left|\frac{-i}{\omega_{\mathrm{L,H}}C}\right|\left|\frac{1}{Z(\omega_{\mathrm{L,H}})}\right| = \frac{1}{\omega_{\mathrm{L,H}}C}\left|\frac{1}{Z_{\mathrm{s}}} - \frac{i}{X_{\mathrm{m}}(\omega_{\mathrm{L,H}})}\right| \;. \tag{A.11}$$

After some rearrangements, the result is

$$G_V(\omega_{\mathrm{L,H}}) = \frac{\omega_0}{\omega_{\mathrm{L,H}}}\sqrt{\frac{R}{Z_{\mathrm{s}}}}Q = \frac{\omega_0}{\omega_{\mathrm{L,H}}}G_V(\omega_0) \;. \tag{A.12}$$

Since $\omega_{\mathrm{L}} \lesssim \omega_0 \lesssim \omega_{\mathrm{H}}$, the opposite relation holds for the gain: $G_V(\omega_{\mathrm{L}}) \gtrsim G_V(\omega_0) \gtrsim G_V(\omega_{\mathrm{H}})$. Even if the matching was not done at resonance, the voltage gain is still as high as the maximum obtainable (actually, the resonance was forced to move where the matching was done). An example of this effect can be found in Fig. A.1
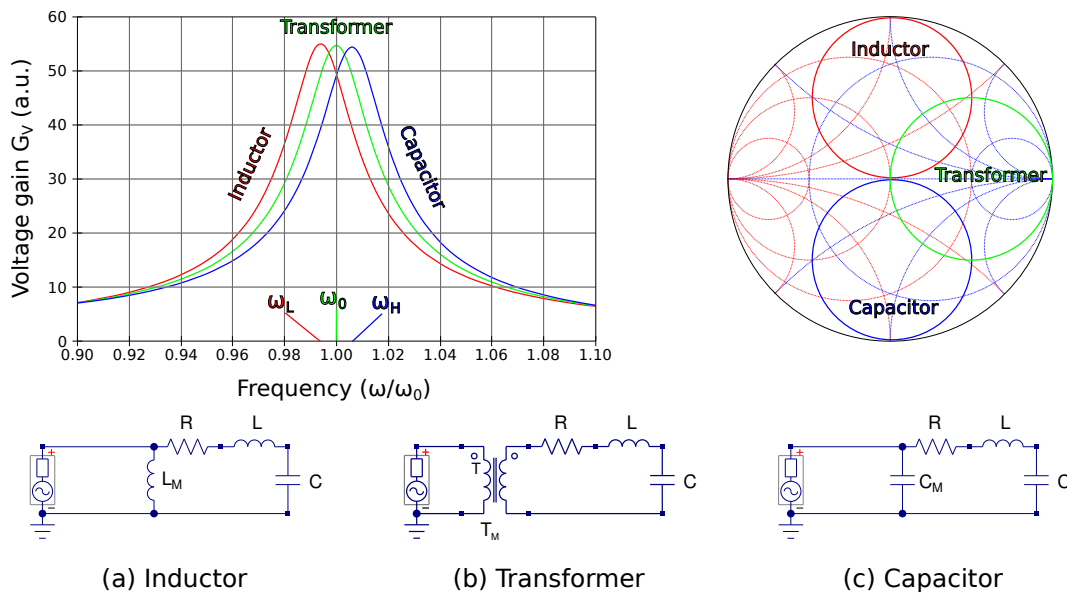
Figure A.1: When matching with only one reactance, it is necessary to match at a different frequency than the resonance. Nevertheless, the voltage gain is not affected significantly since the resonance follows the matching.

References

[1] A. Steane, *Quantum computing*, Rep. Prog. Phys. **61**, 117 (1998).

[2] M. A. Nielsen and I. L. Chuang, *Quantum Computation and Quantum Information*, Cambridge University Press (2004).

[3] R. Blatt and D. Wineland, *Entangled states of trapped atomic ions*, Nature **453**, 1008.

[4] R. Blatt, *The quantum revolution - towards a new generation of supercomputers*, in *Proc. of the XVIII Int. Conf. on Laser Science (ICOLS) 2007*, pages 207–215, (2007).

[5] R. Feynman, *Simulating physics with computers*, Int. J. Theoret. Phys. **21**, 467 (1982),

[6] S. Lloyd, *Universal quantum simulators*, Science **273**, 1073 (1996).

[7] B. P. Lanyon, J. D. Whitfield, G. G. Gillett, M. E. Goggin, M. P. Almeida, I. Kassal, J. D. Biamonte, M. Mohseni, B. J. Powell, M. Barbieri, A. Aspuru-Guzik, and A. G. White, *Towards quantum chemistry on a quantum computer*, Nature Chem. **2**, 106 (2010).

[8] M. Johanning, A. F. Varón, and C. Wunderlich, *Quantum simulations with cold trapped ions*, J. Phys. B **42**, 154009 (2009).

[9] R. Gerritsma, G. Kirchmair, F. Zähringer, E. Solano, R. Blatt, and C. F. Roos, *Quantum simulation of the Dirac equation*, Nature **463**, 68 (2010).

[10] L. K. Grover, *Quantum mechanics helps in searching for a needle in a haystack*, Phys. Rev. Lett. **79**, 325 (1997).

[11] P. W. Shor, *Polynomial-time algorithms for prime factorization and discrete logarithms on a quantum computer*, SIAM J. Comp. **26**, 1484 (1997).

[12] S. Gulde, M. Riebe, G. P. T. Lancaster, C. Becher, J. Eschner, H. Häffner, F. Schmidt-Kaler, I. L. Chuang, and R. Blatt, *Implementation of the Deutsch-Jozsa algorithm on an ion-trap quantum computer*, Nature **421**, 48 (2003).

[13] J. Chiaverini, J. Britton, D. Leibfried, E. Knill, M. D. Barrett, R. B. Blakestad, W. M. Itano, J. D. Jost, C. Langer, R. Ozeri, T. Schaetz, and D. J. Wineland, *Implementation of the semiclassical quantum Fourier transform in a scalable system*, Science **308**, 997 (2005).

[14] K. Brickman, P. C. Haljan, P. J. Lee, M. Acton, L. Deslauriers, and C. Monroe, *Implementation of Grover's quantum search algorithm in a scalable system*, Phys. Rev. A **72**, 050306 (2005).

[15] L. M. K. Vandersypen, M. Steffen, G. Breyta, C. S. Yannoni, M. H. Sherwood, and I. L. Chuang, *Experimental realization of Shor's quantum factoring algorithm using nuclear magnetic resonance*, Nature **414**, 883 (2001).

[16] B. P. Lanyon, T. J. Weinhold, N. K. Langford, M. Barbieri, D. F. V. James, A. Gilchrist, and A. G. White, *Experimental demonstration of a compiled version of Shor's algorithm with quantum entanglement*, Phys. Rev. Lett. **99**, 250505 (2007).

[17] D. P. DiVincenzo, *The physical implementation of quantum computation*, Fortschr. Phys. **48**, 771 (2000).

[18] R. Hughes, T. Heinrichs, and et.al., *Quantum information science and technology roadmap*, (2004) *ARDA*, Report of the Quantum Information Science and Technology Experts Panel http://qist.lanl.gov/qcomp_map.shtml, (2011.06.01).

[19] A. M. Steane, *How to build a 300 bit, 1 giga-operation quantum computer*, in *Quantum Information and Computation*, volume 7, pages 171–183, (2007).

[20] T. Monz, P. Schindler, J. T. Barreiro, M. Chwalla, D. Nigg, W. A. Coish, M. Harlander, W. Hänsel, M. Hennrich, and R. Blatt, *14-qubit entanglement: Creation and coherence*, Phys. Rev. Lett. **106**, 130506 (2011).

[21] D. Kielpinski, C. Monroe, and D. J. Wineland, *Architecture for a large-scale ion-trap quantum computer*, Nature **417**, 709 (2002).

[22] T. Schaetz, D. Leibfried, J. Chiaverini, M. Barrett, J. Britton, B. DeMarco, W. Itano, J. Jost, C. Langer, and D. Wineland, *Towards a scalable quantum computer/simulator based on trapped ions*, Appl. Phys. B **79**, 979 (2004).

[23] J. Chiaverini, R. B. Blakestad, J. Britton, J. D. Jost, C. Langer, D. Leibfried, R. Ozeri, and D. J. Wineland, *Surface-electrode architecture for ion-trap quantum information processing*, arXiv:0501147v2 [quant-ph] (2005).

[24] J. Labaziewicz, Y. Ge, P. Antohi, D. Leibrandt, K. R. Brown, and I. L. Chuang, *Suppression of heating rates in cryogenic surface-electrode ion traps*, Phys. Rev. Lett. **100**, 013001 (2008).

[25] W. MacAlpine and R. Schildknecht, *Coaxial resonators with helical inner conductor*, Proc. of the IRE **47**, 2099 (1959).

[26] W. Paul, *Electromagnetic traps for charged and neutral particles*, Rev. Mod. Phys. **62**, 531 (1990).

[27] G. Werth, N. G. Viorica, and G. M. Fouad, *Charged Particle Traps II: Applications*, Springer (2009).

[28] H. G. Dehmelt, *Radiofrequency spectroscopy of stored ions i: Storage*, Advances in Atomic and Molecular Physics **3**, 53 (1968).

[29] C. Champenois, *About the dynamics and thermodynamics of trapped ions*, J. Phy. B **42**, 154002 (2009).

[30] J. T. Barreiro, M. Müller, P. Schindler, D. Nigg, T. Monz, M. Chwalla, M. Hennrich, C. F. Roos, P. Zoller, and R. Blatt, *An open-system quantum simulator with trapped ions*, Nature **470**, 486 (2011).

[31] M. Harlander, R. Lechner, M. Brownnutt, R. Blatt, and W. Hänsel, *Trapped-ion antennae for the transmission of quantum information*, Nature **471**, 200 (2011).

[32] R. J. Hughes, D. F. V. James, E. H. Knill, R. Laflamme, and A. G. Petschek, *Decoherence bounds on quantum computation with trapped ions*, Phys. Rev. Lett. **77**, 3240 (1996).

[33] H. Miller, *Surface flashover of insulators*, IEEE Trans. El. Ins. **24**, 765 (1989).

[34] M. Brownnutt, G. Wilpers, P. Gill, R. C. Thompson, and A. G. Sinclair, *Monolithic microfabricated ion trap chip design for scaleable quantum processors*, New J. Phys. **8**, 232 (2006).

[35] D. Sigg, *Printed circuit boards for ultra high vacuum*, LIGO Technical Notes (2006), http://ific.uv.es/elec/files/PCB-UHV.pdf (2011.06.01).

[36] R. W. Rhea, *HF Filter Design and Computer Simulation*, Noble Publishing (1994).

[37] A. I. Zverev, *Handbook of Filter Synthesis*, John Wiley and Sons, Inc. (1967).

[38] S. Gulde, *Experimental realization of quantum gates and the Deutsch-Josza algorithm with trapped ^{40}Ca-ions*, PhD thesis, University of Innsbruck (2003).

[39] P. L. D. Abrie, *Design of RF and Microwave Amplifiers and Oscillators*, Artech House Publishers (1999).

[40] J. W. Ekin, *Experimental Techniques for Low-Temperature Measurements*, Oxford University Press (2006).

[41] M. D. Hughes, B. Lekitsch, J. A. Broersma, and W. K. Hensinger, *Microfabricated Ion Traps*, arXiv:1101.3207 [quant-ph] (2011).

[42] R. Dubessy, T. Coudreau, and L. Guidoni, *Electric field noise above surfaces: A model for heating-rate scaling law in ion traps*, Phys. Rev. A **80**, 031402 (2009).

[43] R. J. Epstein, S. Seidelin, D. Leibfried, J. H. Wesenberg, J. J. Bollinger, J. M. Amini, R. B. Blakestad, J. Britton, J. P. Home, W. M. Itano, J. D. Jost, E. Knill, C. Langer, R. Ozeri, N. Shiga, and D. J. Wineland, *Simplified motional heating rate measurements of trapped ions*, Phys. Rev. A **76**, 033411 (2007).

[44] J. Labaziewicz, Y. Ge, D. R. Leibrandt, S. X. Wang, R. Shewmon, and I. L. Chuang, *Temperature dependence of electric field noise above gold surfaces*, Phys. Rev. Lett. **101**, 180602 (2008).

[45] J. Cox, *Iron powder cores for high Q inductors*, Micrometals, Inc. technical report, http://www.micrometals.com/appnotes/appnotedownloads/ipc4hqi.pdf, (2011.06.01).

[46] E. Gao, S. Sahba, H. Xu, and Q. Ma, *A superconducting RF resonator in HF range and its multi-pole filter applications*, IEEE Trans. Appl. Super. **9**, 3066 (1999).

[47] F. Huang and X. Xiong, *Very compact spiral resonator implementation of narrowband superconducting quasi-elliptic filters*, in *33rd European Microwave Conference*, pages 1059 –1062 (2003).

[48] E. Belohoubek, D. Kalokitis, A. Fathy, E. Denlinger, A. Piqué, X. Wu, S. Green, and T. Venkatesan, *High temperature superconducting components for microwave systems*, App. Superconductivity **1**, 1555 (1993), World Congress on Superconductivity: Proceedings of the 3rd International Conference and Exhibition.

Acknowledgements